



UNIVERSITÀ DEGLI STUDI DI PADOVA

DIPARTIMENTO DI INGEGNERIA INDUSTRIALE

CORSO DI LAUREA MAGISTRALE IN INGEGNERIA DELL'ENERGIA ELETTRICA

Tesi di Laurea Magistrale in

Ingegneria dell'Energia Elettrica

Technological development activities for a VRFB- Industrial Size Test Facility

Relatore: Prof. Piergiorgio Alotto

Correlatore: Ing. Andrea Trovò

Laureando: Alessandro Sutto

ANNO ACCADEMICO 2017 – 2018

Abstract

This thesis focuses on both scientific and experimental activities developed to implement the control and the maintenance of the Vanadium Redox Flow Battery Industrial Size test facility based in the Energy Storage Laboratory in the University of Padova. The main activity consisted in enhancing the LabVIEW management software by introducing automatic routines to plot polarization curves, to compute efficiencies and by making the user interface more user-friendly. The collected data are here presented. Preliminary studies on an advanced temperature control were also conducted and are here reported. The main task of the experimental work was devoted to the activities of Maintenance, Repair and Operations to check the status of the plant after one year of operation. Other minor experimental labor was the installation of devices to ensure the safety to the plant, to reduce electromagnetic interferences and to extend the admissible load range.

Index

Abstract	iii
1 Introduction	1
1.1 Energy Storage Technologies	1
1.2 Vanadium Redox Flow Batteries	3
1.2.1 Main Features – Pros and Cons.....	3
1.2.2 Reactions and Electrolytes	4
1.2.3 General Structure	6
1.2.4 Electrodes.....	9
1.2.5 Membrane.....	9
1.3 Costs Comparison.....	9
2 Energy Storage Lab Device and Equipment	13
2.1 The Battery	14
2.2 The Measurement and Control System	16
2.2.1 Sensors	17
2.2.2 Electric Power and Measurement Circuits.....	20
2.2.3 Security devices and measures	24
2.3 Electromagnetic interference protection	26
2.4 LabVIEW acquisition system	29
2.4.1 LabVIEW Block Diagram	30
2.4.2 LabVIEW Front Panel.....	33
2.5 LabVIEW Ancillaries.....	35
2.5.1 LEM Current Transducer Calibration SubVI.....	36
2.5.2 OCV to SOC SubVI.....	38
2.5.3 Integral Efficiency SubVI.....	40
2.5.4 α -factor SubVI	42

3	Polarization Curves.....	45
3.1	Passive load construction and cabling	46
3.2	LabVIEW and Matlab Automation.....	49
3.3	Results	54
4	Efficiency	59
4.1	LabVIEW Automation	59
4.2	Results	63
5	Temperature Control.....	65
6	Aging Effects and MRO	69
6.1	Dismantling and check operations	69
6.2	Reassembly operations	76
7	Conclusions.....	81
8	Figure Index.....	83
9	Nomenclature.....	87
10	Bibliography.....	89

1 Introduction

1.1 Energy Storage Technologies

Electrical energy production and consumption has grown significantly in the last decade as a result of the huge electrical penetration in lots of everyday life activities and of the rapid development of an increasing number of countries. It has reached $20 \cdot 10^3$ TWh/yr and it keeps growing at a rate of 3%/yr [1] with significant adoption of Renewable Energy Sources (RESs) mainly photovoltaic (PV) and Wind technologies.

As it is known, RESs are not as predictable in power production as the fuel-based conventional technologies. On the contrary they are characterized by a strong variability depending on several factors that can't be totally handled or controlled. To overcome this issue, the best solution is to store the produced energy when the demand lowers the production and distribute it when the request gets higher, taking into account both economic and technologic factors. Storage of energy can, indeed, lower the overall costs of distribution of electrical energy. The solutions in this field are a lot and they cover a wide range of possibilities. Every storage technology is characterized in terms of power and energy capacity, response time, capacity loss rate, efficiency, scalability, stand-alone or isolated configuration compatibility and more.

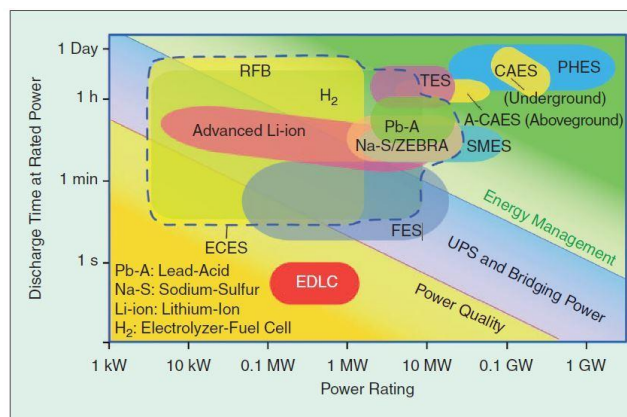


Figure 1.1 Graphical representation of Discharge Time vs. Power for the main ES technologies. Some of them are already available other are under development. [1]

Figure 1.1 shows a diagram where the possible technologies for Electrical Energy Storage are organized according to the discharge time at rated power versus power rating. The diagram is divided into three zones: Power Quality zone in the bottom left corner, characterized mostly by low discharge time and low power, Energy Management zone in the top right corner, for high

discharge time and power and an intermediate UPS (uninterruptable power supply) and Bridging Power zone.

The mostly used system nowadays for Energy Management is the Pumped Hydro Energy Storage technology (PHES) in which water is pumped up the dams when there is an excess in energy production. Power and energy that can be stored are high and the efficiency of the process can achieve high values. The water (or energy) reservoir can be stored on a time scale that can be of the order of days or weeks. On the other hand, this technology can't be decentralized, and it needs very particular geographic configuration so that it can't be placed everywhere. Moreover, its response is slow, making it not suitable in the case of sudden request of power.

A more fitted technology that can be better coupled with RESs is represented by the Electro Chemical Energy Storage (ECES) systems. They are set in an intermediate level of storage and their main feature is that they can easily be employed in the case of intermittent production but continuous request of electricity. As part of this category there are Li- or Na-based batteries, Pb-acid batteries, supercapacitors, Fuel cells or H₂-based technologies and Redox Flow Batteries (RFBs). The latter is a kind of technology which in the last years has risen a particular interest out of the scientific community for its promising features.

In recent years, because of the rapid development in the battery industry, the demand started growing and the technologies has reached a high level of differentiation and specification to better answer the peculiarity of its employment. Four big areas of employment can be distinguished among batteries: Automotive SLI (Starter, Lights, Ignition) totally occupied by Pb-Acid, Automotive Traction, Consumers Electronics and Stationary Storage. CAIRN Energy Research Advisor has forecasted a global growth in the battery market for the next years passing from the 2013 47.7 GWh to 96.6 GWh in 2020, reaching almost \$24 billion of revenue mostly concentrated in Asia and Europe. Regarding the Stationary Storage part, CAIRN evaluated that the biggest improvement will be in the grid management and in the peak shifting service where high energy and power batteries will be employed more and more. Both services will rise their revenue from nowadays hundreds of millions of dollars to more than \$1.2 billion in 2020. Grid management is supposed to reach almost 1 GWh of battery supply and peak shifting to overcome 6.5 GWh. [2]

Redox Flow batteries are (and will be) used at medium-high level of storage and mostly for load levelling or power quality control as far as a support to RESs.

RFB technology is set in between electrochemical secondary batteries and fuel cells. As the batteries, the same device can be used for both charging and discharging and all the electrochemically active species are in a liquid form and they are stored inside the sealed battery tank. But as in the fuel cells, the electroactive species are inside the electrolyte instead of the electrodes. The electrodes are the active sites of the battery, that is the place where Redox

reactions occur. They must be separated by an ion-permeable membrane and they must be connected to an external electrical circuit in order to allow the charges to move and let the reactions take place. The overall structure is very similar to that of a Fuel Cell based on a Membrane Electrode Assembly (MEA) block architecture. To get higher values of voltage than the one expressed by the involved reactions, cells are connected in series in stack configuration separated by bipolar plates. The modular structure is one of the strongest advantage of this technology, making its design suitable for both small or big power plants as well as for power supply for small buildings or grid management.

1.2 Vanadium Redox Flow Batteries

1.2.1 Main Features – Pros and Cons

Among the RFBs, the most promising are the all-Vanadium or VRFBs. As all the other RFB, they have high flexibility in the design considering the independent sizing of power and energy. In fact, power depends on the size of the active area where the electrolyte reacts and on the number of cells in the stack, while energy depends on the concentration of the electrolytic solutions and the size of the tanks which contain them. By rising these values, both power and energy will increase. Moreover, they don't set any geographical limit giving the possibility to be installed almost everywhere. Their environmental footprint is very low. Scaling them up or down is very easy. They present high values of efficiency, fast responsiveness and complete reversibility. They can both withstand high Deep of Discharge (DoD) or being overloaded for short periods of time. That means that the battery can be totally discharged with no detriments of materials or performances' problem in further cycles. [3]

There is no necessity of ancillary cooling or heating systems because the working temperature floats around room temperature even though thermal management is critical to ensure long life. The storage system needs temperature monitoring in order to keep it in a range in which no precipitation of electrolyte occur. As it will be shown later in this thesis (§5), the thermal control can be simply performed by periodic recirculation of electrolyte solutions in the stack.

VRFBs have a very low self-discharge rate and the electrolyte can be reused almost forever once sealed in the tanks. It has been shown that with an adequate mix of solvers, temperature control and periodic remixing, the precipitation in the electrolyte is avoided giving the possibility of recycling it almost indefinitely [4]. Moreover, being both electrolytes based on Vanadium ions solutions, the cross-contamination is lowered significantly. Once the battery is charged and there is no more electrolyte in the active sites, the battery keeps its charge in the tanks for a very long time.

It has been demonstrated that its responsiveness is very fast, in the order of milliseconds, but the charge can be kept and given during hours as well, making this technology suitable spanning from power quality control to energy management. The storage of electrolyte in fact is very safe, it can be kept inside plastic tanks with no specific requirement and in case of leakage it can be poured again inside the device (if it hasn't been contaminated) with no losses in terms of efficiency or quality [3].

However, VRFBs present a strong and limiting drawback in their low values of power and energy densities. The latter in particular mainly restricts the technology from spreading because it's not competitive with other more advanced technologies. Nowadays energy densities float around 10-35 Wh/kg or 25 Wh/l which is around ten times lower of a Li-based battery. The concentration of the electrolyte is the main responsible for this low value forcing to use big tanks and volumes of solutions to store energy. Just recently it has been demonstrated that highly concentrated solution can be kept stable at the same range of temperature [4] raising the energy density value. Further improvements can be achieved by developing more efficient membranes that can reduce the crossover effect as well as adding some sort of catalyst on the electrodes to enhance the reactions. Additionally, it presents side reactions which may cause loss of capacity over extended cycling. In particular, V(II) is sensitive to oxygen and it should be kept as much as possible in a protected atmosphere to avoid precipitation. As previously said precipitation will occur in other species as well (in the positive electrolyte V_2O_5 precipitates for $T > 50^\circ\text{C}$ and in the negative $(VO)SO_4$ for $T < 10^\circ\text{C}$) calling for an adequate temperature control. Moreover, since the electrolytes are conductive, they will present shunt currents along the distribution channels which affect the overall efficiency. If the cells have a large active area, the overall occupied volume is high, and it causes transverse gradient of solutions flowing towards the active sites of the electrodes reducing efficiency. [3]

1.2.2 Reactions and Electrolytes

Vanadium is a rare transition metal mostly employed for some special steel production. It is present in several minerals and can be rarely found pure in nature. It's produced mostly as a by-product in steel production from steel smelter slag or from the flue dust of heavy oil or even from uranium mining. All its compounds are classified as toxic and the United States National Institute for Occupational Safety and Health (NIOSH), classified some of them as immediately dangerous to life and health because they are likely to cause permanent health problems or death. Vanadium based electrolytes are quite corrosive so that metal parts in the battery equipment must be avoided. That means pipes, pumps and tanks must be produced using plastic or compound materials.

VRFBs exploit the four oxidation states of Vanadium. V(II)/V(III) and V(IV)/V(V) couples in sulfuric acid or sulphate-chloride mixed solvent are used as negative and positive electrolyte respectively.

The electrochemical reactions during charge and discharge are as follows:

Positive electrode reaction:



$$E_c^0 = 1.004 V \quad (2)$$

Negative electrode reaction:



$$E_a^0 = -0.255 V \quad (4)$$

The overall electrochemical reaction is



$$OCV = 1.259 V \quad (6)$$

When the battery is fully charged, there are just ions with V(V) and V(II) vanadium in the solutions, and, as the battery is discharged they are converted into V(IV) and V(III). Each of these oxidation state is characterized by a peculiar colour (V(II) purple, V(III) green, V(IV) blue, V(V) yellow) so that colours can give a preliminary information over the State of Charge (SOC) of the battery by simply looking at the solutions in the tanks. More precise methodology that involve titration or advanced spectroscopy can successfully be implied in the measurement of SOC, but the latter's cost is high and its calibration very difficult compared to others.

It was demonstrated that the SOC and the cell voltage are strictly related so that to obtain information on the charge left in the device, a simple measurement of the open circuit voltage is

enough. Other and more sophisticated methods have been investigated: some of them regards the already cited spectroscopy of the solutions using absorbance, others regard the variation in the conductivity of the different solutions. All these can be incorporated in the management system giving the possibility of scheduling electrolyte rebalancing procedures such as periodic remixing to restore the full capacity and to ensure a long-term efficient operation of the battery [5].

Even if the energy capacity of the system increases with the concentration of vanadium salts, electrolyte solutions must not overcome their solubility limits in order not to enhance the precipitation. As the solubility varies with the temperature it's important to set some limits in the working range. It has been demonstrated and long investigated since the 1980s, that if the working conditions floats between +10 to +50 °C precipitation is avoided with molarity of vanadium as high as 2.5 M [6].

Using a mixed sulphate-chloride solution for electrolyte, there should be the possibility of chlorine gas evolution but under normal conditions vanadium oxidation occurs before chlorine oxidation. Even in the case of its production it would dissolve in the solutions, given its relatively high solubility. [4]

1.2.3 General Structure

From the chemical reactions, a value of OCV (Open Circuit Voltage) of 1,26 V is obtained which is not enough to make a single cell work coupled with high values of power and energy so that a stack configuration is necessary.

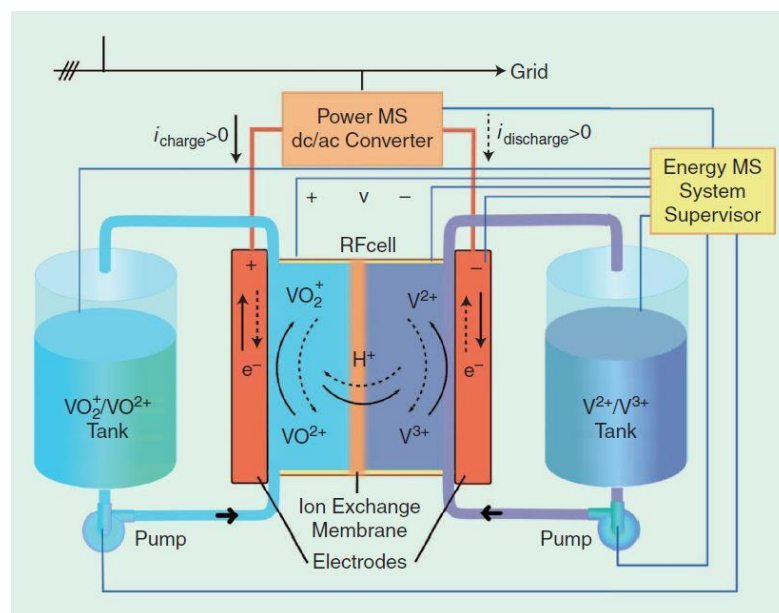


Figure 1.2 General structure of a VRFB cell with all its fundamental components. [1]

Figure 1.2 shows the general structure of a VRFB. There are two tanks from which by two different pumps, the electrolytes are pumped in the central MEA-like structure where the reactions occur. A pipe system for the circulation of the solutions and an external circuit for the circulation of electrons, from which power is extracted, are needed. A Management System (MS) is required as well to supervise the battery activities and parameters. Moreover, Power Electronics devices can be present to complete the set up in order to couple the battery with the grid or eventually the energy sources.

As previously said, all the structural parts must be made of plastic and they must ensure watertight seal not to let vanadium compounds leak out. This ensure a long life-time and low maintenance requirement. Plastic materials like PVC (Polyvinyl Chloride) which are cheap and largely available in the markets, can be used as construction material with no need of special plastics.

The MEA is the core of the battery and it's where the most improvement for battery efficiency can be done. The stack configuration is composed of several layers where ions conductive membranes are interposed to electrodes coupled with electric conductive bipolar plates. At the end of the stack, metal current collectors ensure electrical conduction to the system.

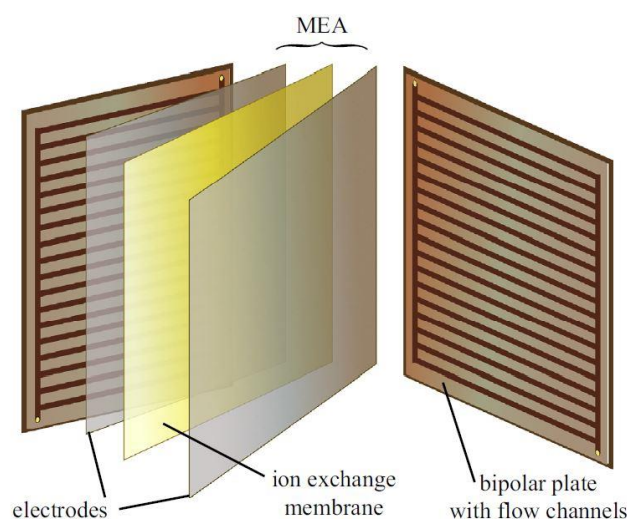


Figure 1.3 The MEA. A single cell's structure. [3]

Figure 1.2 shows the typical and cheaper *Batch Recirculation* operation mode for a RFB. In this configuration, each of the electrolytes circulates between one of the stack and a dedicated tank. In this way a uniform concentration is maintained for both anolyte and catholyte tanks but changes gradually for each species during charge and discharge [7].

Independently of the mode of operation VRFB stacks can be characterized by their feeding mode.

- Parallel Feeding: The stack of cells is arranged as in Figure 1.4 where all the modules operate with the same inlet and the electrolyte is then distributed to all the cells via an internal manifold system. In this way all the cells work with the same concentration of active species and a similar volumetric flow rate. In order to avoid gas bubbles to stays in the active area, a lower outlet with respect to the inlet is suggested. The main drawback is represented by the formation of shunt currents inside the electrolytes which lower the overall efficiency and can give thermal instability. Anyway, this is the most convenient configuration for both small or medium-size RFBs.
- Series Feeding: The cells are, in this case, arranged in cascade so that the electrolytes flow successively through each of them. That leads to a different concentration of reactants in every cell and to a non-uniform distribution of flow. This method results in a higher pressure drop as well. In theory shunt currents should be avoided [7]. This mode needs for a model which keeps under control the progressive reactants consumption in order to ensure that the final cell in the cascade is not underfed.

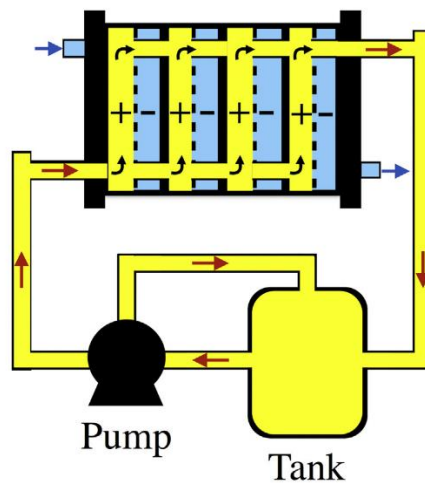


Figure 1.4 Parallel Feeding for a VRFB. It is depicted just the circulation of one of the two electrolytes.

Considering the electrodes, two flow configurations are the most employed.

- Flow-By: the electrical current is perpendicular to the fluid flow. It has economic and practical advantages over other possible configurations. By using porous electrodes, the active area is increased, the mass transport's enhanced and good electrical connection's ensured.

- Flow-Through: the electrical current is parallel to the fluid flow. This configuration is only possible with porous electrodes.

1.2.4 Electrodes

The electrodes are the sites where electrochemical reactions occur, but they don't take part in them directly. To obtain high energy efficiency they must ensure a high electrochemical activity and reversibility for the Redox couples, ensure good conductivity to prevent ohmic losses and have a stable 3D structure with a high specific area providing narrow channels for the electrolytes to wet them. Moreover, they must be chemically, mechanically and electrochemically stable but with a reasonable cost to meet the large-scale production. Carbon-based materials are then chosen. Different prototypes or commercial products show different choices between the available technologies depending on costs versus performances. Carbon felts, adequately carved graphite plates, graphite felts, carbon paper or nano-scaled carbon tubes are some of the technologies that can be employed. Their performances can be modified by adding electrocatalysts species or according to the management of flux of electrolytes or the shape of carving in the solid current collectors [8].

1.2.5 Membrane

The membrane is generally cationic (proton exchange) and the mostly employed material is Nafion from DuPont. This material requires to be wetted by water to become conductive. It can be modified in order to let SO_4^{2-} ions pass but, in this case, cross-contamination between the two solutions would be higher considering that SO_4^{2-} are bigger than protons. This component is the most expensive and the one which undergoes the deeper aging in the cell so that the research is focused on its development to lower the cost and make it more resistant, stable and improve its selectivity.

Over the last decade many research groups started investigating new possibilities for membranes materials. Widespread attention rose around nonfluorinated membranes due to their lower cost and their reduced ion permeability [9]. Of these, the most studied is the sulfonated polyether ether ketone (SPEEK) that not only exhibits high chemical stability in vanadium electrolyte but also has a round-trip DC energy efficiency similar to the one of Nafion. [10]

1.3 Costs Comparison

Several studies ([11], [12], [13]) have been conducted about the pricing of a VRFB stack and/or plant. Some of them were focused just on the price of raw construction materials to try to find convenient alternatives. Others took into account the whole plant's costs in order to estimate a range of final price for electricity to be produced or sold. Others made a Life Cycle Analysis

comparing this technology with other already present in the market. The past years investigation is very vast and detailed presenting a rich set of data and analysis. Here are reported some significant results just to present a summary.

Table 1.1 shows the costs for the raw materials that constitute the active part of the cell. As it can be seen the membrane is the most expensive raw material. Excluding it, the rest of the materials are very cheap. In fact, as previously said the researcher are nowadays interested in the study of membranes to make them cheaper, more resistant and more efficient.

MATERIAL	YEAR 2014 COST	
Negative solution (V)	[\$ /kg]	29
Positive solution (V)	[\$ /kg]	29
Electrolyte (H ₂ SO ₄)	[\$ /kg]	0.1
Graphite for flow field plate	[\$ /kg]	7
Carbon felt electrodes	[\$ /m ²]	70
Membrane	[\$ /m ²]	500
Frames, seals and total manifolds	[\$ /m ²]	6
BOP		
(Balance of Plant)	[\$ /kW]	410

Table 1.1 Material costs of raw materials for a VRFB stack based on the 2015 analysis by Seungbum Ha et al. [11]

Figure 1.5. shows in a histogram the breakdown for materials, purchased items and ancillaries costs needed for a plant to be put on operation. The investigation by Seungbum Ha et al. considers the cost relative to the 2014 with a simulated production rate of 20,000 stacks/year. [11] It can be noticed that the positive and negative solvents as well as the membrane constitutes almost the half of the price.

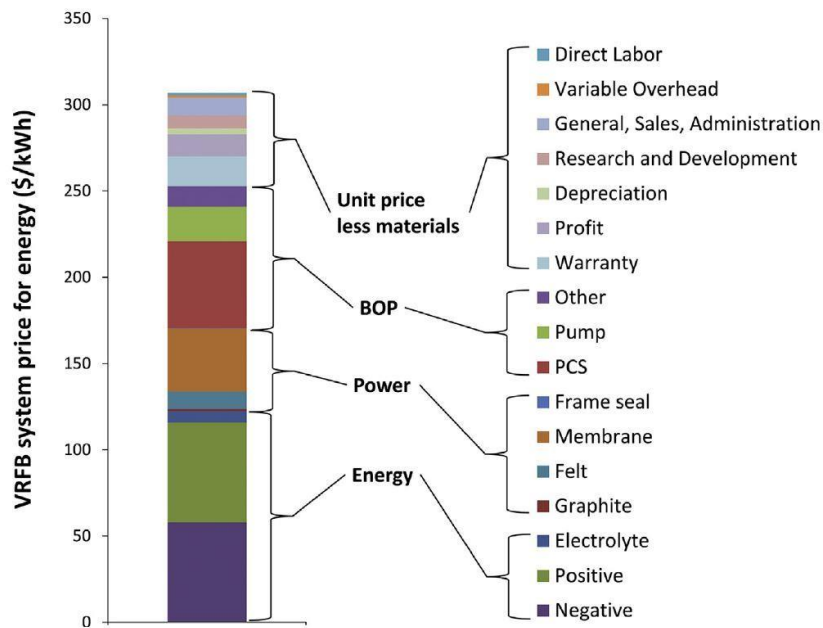


Figure 1.5 . VRFB costs breakdown for materials and ancillaries. [11]

Considering the whole plant operation, a mayor scale analysis was performed by Behnam Zakeri et al. [13] presenting a meticulous bibliographic review where they critically examine the existing literature about the life cycle costs and provide an update database for the cost elements for several energy storage technologies. Table 1.2. shows their results regarding VRFB.

COST ITEM	AVERAGE	
PCS ^a	[€/kW]	490
Storage section ^b	[€/kWh]	467
Fixed O&M	[€/kW-yr]	8.5
Variable O&M	[€/MWh]	0.9
Replacement costs ^c	[€/KW]	130

Table 1.2 Main cost items of VRFB system. a) Including BOP = 25 €/kW. b) For MW size plants with DoD of 80% and T&D support (4h discharge time). c) Every 8 yr considering (356 to 500 cycles/yr). [13].

With the collected data Behnam Zakeri et al. presented a good comparison between several energy storage technologies spacing through all the power range [13]. The results are shown in Table 1.3. The highlighted row is the one relative to VRFB. It can be noticed once again the high

flexibility of this technology regarding the power range which can vary from kW to MW and regarding the discharge time (from seconds to hours). Its efficiency can be compared to the one of PHES that is one of the most developed storage solution nowadays. Other pros listed before are durability of capacity that can reach months and the low self-discharge. The main drawbacks are represented by the low power and especially energy density which are, at the moment, not competitive with other electrochemical commercial technologies like Li-based batteries.

Technical characteristics of electrical energy storage (EES) systems.

EES technology	Power range (MW)	Discharge time (ms-h)	Overall efficiency	Power density (W/kg)	Energy density (Wh/kg)	Storage durability	Self-discharge (per day)	Lifetime (yr)	Life cycles (cycles)
PHS	10-5000	1-24 h	0.70-0.82		0.5-1.5	h-months	Negligible	50-60	20000-50000
CAES (underground)	5-400	1-24 h	0.7-0.89		30-60	h-months	Small	20-40	> 13,000
CAES (aboveground)	3-15	2-4 h	0.70-0.90			h-days	Small	20-40	> 13,000
Flywheel	Up to 0.25	ms-15 m	0.93-0.95	1000	5-100	s-min	100%	15-20	20,000-100,000
Lead-acid	Up to 20	s-h	0.70-0.90	75-300	30-50	min-days	0.1-0.3%	5-15	2000-4500
NaS	0.05-8	s-h	0.75-0.90	150-230	150-250	s-h	20%	10-15	2500-4500
NaNiCl ₂ (ZEBRA)	50	2-5 h	0.86-0.88	150-200	100-140	s-h	15%	15	2500-3000
Ni-Cd	Up to 40	s-h	0.60-0.73	50-1000	15-300	min-days	0.2-0.6%	10-20	2000-2500
Li-ion	up to 0.01	m-h	0.85-0.95	50-2000	150-350	min-days	0.1-0.3%	5-15	1500-4500
VRFB	0.03-3	s-10 h	0.65-0.85	166	10-35	h-months	Small	5-10	10,000-13,000
Zn-Br	0.05-2	s-10 h	0.60-0.70	45	30-85	h-months	Small	5-10	5000-10,000
Fe-Cr	1-100	4-8 h	0.72-0.75					10-15	> 10,000
PSB	15	s-10 h	0.65-0.85			h-months	Small	10-15	2000-2500
SMES	0.1-10	ms-8 s	0.95-0.98	500-2000	0.5-5	min-h	10-15%	15-20	> 100,000
Capacitors	Up to 0.05	ms-60 m	0.60-0.65	100,000	0.05-5	s-h	40%	5-8	50,000
SCES	Up to 0.3	ms-60 m	0.85-0.95	800-23,500	2.5-50	s-h	20-40%	10-20	> 100,000
Hydrogen (fuel cell)	0.3-50	s-24 h	0.33-0.42	500	100-10,000	h-months	Negligible	15-20	20,000

Table 1.3 Technical characteristics of EES systems.

To conclude, a capex (capital expenditure) was computed resulting < 4.4 c€/kWh-cycle inclusive of ancillaries and based on contracts of 2015 [1]. This was the cheapest among the considered EES technologies (Advanced Pb-acid, Na-S, Na-Ni-Cl, Li-ion, FCs, VRFB).

2 Energy Storage Lab Device and Equipment

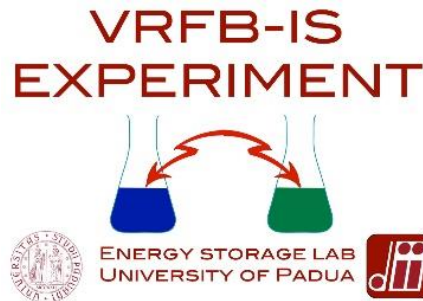


Figure 2.1 Vanadium Redox Flow Battery - Industrial Scale Experiment logo.

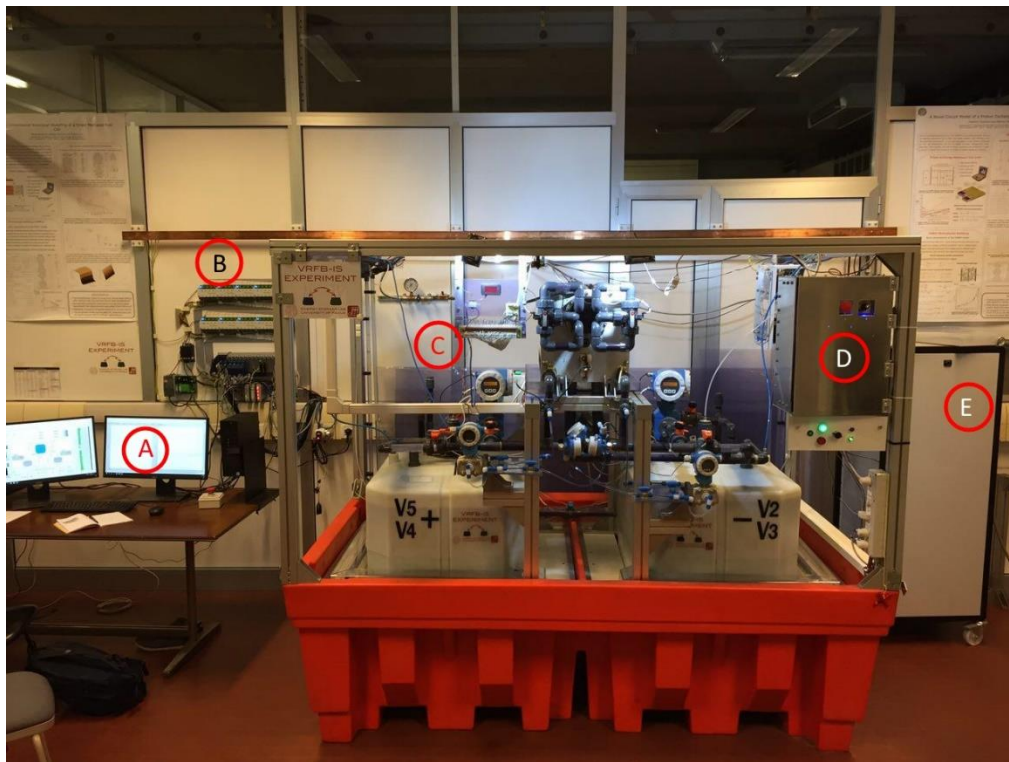


Figure 2.2 Energy Storage Lab VRFB-IS main components. A) the Computer with the LabVIEW software user interface, B) opto-isolators, CompactDAQ and other acquisition instruments, C) the VRFB test facility complete with all the measurement equipments, D) Electric panel and power sink selector panel, E) the power supply.

The Energy Storage Lab (ESLab) is set in the Industrial Engineering Department of the University of Padua. This thesis work is part of the *VRFB-IS EXPERIMENT*. The experiment aims to develop a

state-of-the-art Vanadium Redox Flow Battery and consists of a campaign of studies on a fully-monitored domestic-industrial sized test facility prototype focused on the optimization of its performances, creating a user-friendly interface to acquire signals and control them and on researching over a wide range of peculiarity of this technology (e.g. modelling, thermal behaviour, electrolytes stability, materials aging effects and more).

Differently from other research groups, the plant in the ESLab has industrial scale, so that it opens a new area in the research of this technology which main way out is represented by the large scale electrical energy storage. The whole plant is composed by the battery components (i.e. tanks, stack, pipes etc.), an independent DC power supply, the measure equipment (described in §2.2) a computer for the data acquisition through a LabVIEW interface and some other apparatus that will be presented further in this work. Some data and dimensions of the plant are reported in Table 2.1.

Rated Power ^a	3,6	kW
Rated Energy	25	kWh
Rated Current ^a	72	A
Voltage Range	40 – 60	V
Number of Cells	40	
Total Active Area	600	cm ²
Tank capacity	1000 (500x2)	dm ³
Electrolytes		
Sulfuric acid concentration	4,5	mol/dm ³
Vanadium concentration	1,6	

Table 2.1 Characteristics of the plant. a) these values were the ones declared by the stack producer, but recent experiments have increased their value.

2.1 The Battery

The battery is composed by 40 cells electrically connected in series but fed in parallel by the electrolytes. Each cell is an assembly made of a graphite bipolar plat, a carbon felt and Nafion 212 membrane. The membrane is sealed with a gasket to prevent any leakage while the bipolar plates are sustained by a plastic structure suitably carved with manifolds to guide the electrolyte to the electrodes. The total active area is 600 cm². The electrolytes are two solutions of 1,6 M of vanadium salts solved in 4,5 M aqueous solution of sulfuric acid. They're stored in two separate tanks (one for the anolyte and one for the catholyte) each with a capacity of 500 l and they're

pumped to the stack by two magnetic driven motors through a hydraulic pipe plant. The latter's furnished with several manual valves that can regulate the fluxes and/or exclude some part of the entire battery. For example, when the battery is not working the stack can be isolated in order to maintain the electrolytes inside the cells or, on the contrary, it can be totally emptied. A particular feature of the plant is a pipe directly connecting the two tanks that can be opened or closed by a valve and that is used to rebalance the volumes of anolyte and catholyte when their drop exceeds a critical point. In all the components, metal parts are little employed because of the corrosive acid working environment. In particular, all the pipe system is made of PVC.

On the front head of the stack, a single separate cell is mounted and fed by the same electrolyte flowing inside the active cells. This is electrically isolated and it's used to obtain the Open Circuit Voltage of the system from which the State of Charge of the battery can be computed as will be shown in §2.5.2. Above it, there's a system of valves that can be set to remix the two electrolytes and restore the initial capacity stored in the solutions and lost for the crossover effect.

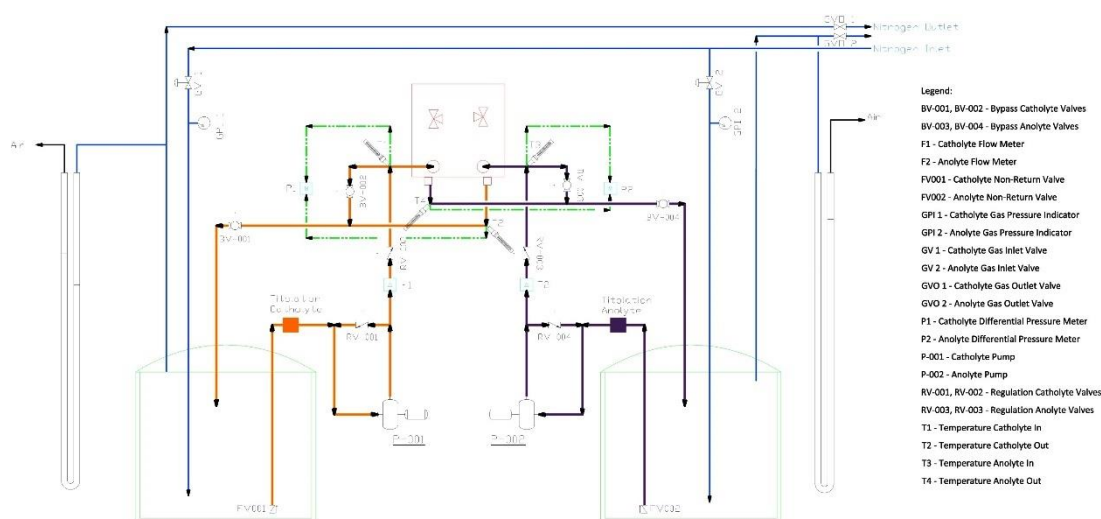


Figure 2.3 P&ID of the hydraulic plant in detail.

Lastly two innovative differential water pressure gauges are installed connected to an external nitrogen source to perform a triple role:

- They easily and visually give an approximate information about the pressure present inside each tank with respect to the atmospheric level.
- They successfully protect the tank from overpressures by simply expelling the water after 1 bar of difference is reached.
- They effectively seal the tanks preventing air (i.e. oxygen) to enter them and provoke undesired oxidation reactions.

Figure 2.3 is the complete P&ID diagram of the hydraulic plant. Figure 2.4 represents the structure of the pressure gauges in detail where the dotted orange part is nitrogen, the dotted blue represents water and the dotted grey is air.

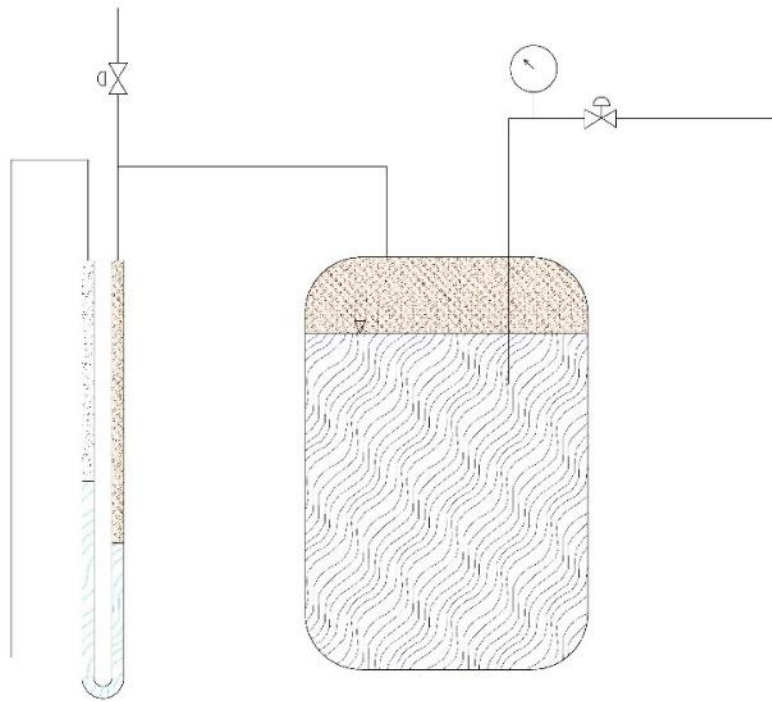


Figure 2.4 Differential pressure gauge detail.

2.2 The Measurement and Control System

Apart from the electrochemically active part of the VRFB plant, a complex and dedicated measurement system was equipped to fully-monitor the state of the battery. It is composed by some sensors described later and an acquisition system for all the signal handled by a LabVIEW interface. Controls through analogic outputs of a NI CompactDAQ are performed. A PLC and some others security devices are installed to ensure intrinsic safety to the whole plant as described later in §2.2.3.

In Figure 2.5 from top to bottom it can be seen the copper equipotential grounding bar, the opto-isolators, the CompactDAQ with all its modules and connections and the Programmable Logic Controller. This complex apparatus was installed only for research purpose indeed a real commercial industrial-size VRFB will be smaller and more compact.

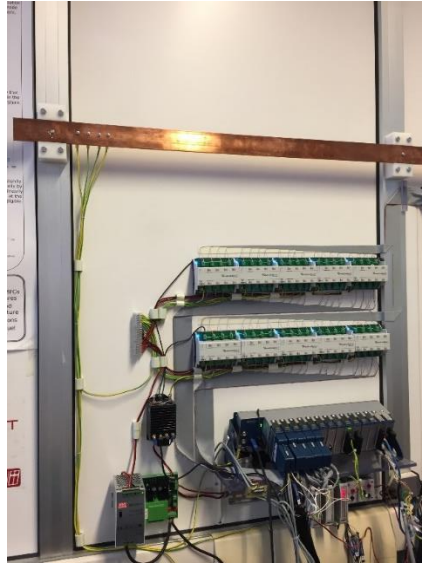


Figure 2.5 Acquisition core system.

2.2.1 Sensors

In this chapter a brief description of the measurement equipment including sensors and support apparatus, are presented.

- **Volumetric Flow:** Figure 2.6 shows one of the two installed Endress+Houser Proline Promag 50 volumetric flow meter. The plant is furnished with two of these meters, one for each electrolyte, installed downstream of the pumps and upstream of the stack. Its signal is a current output proportional to the flow. Its range spaces between 4 to 20 mA. The signal is lead to the NI 9207 module of the compactDAQ throughout a shielded cable. The instruments have a dedicated supply line distinguished from the measure.



Figure 2.6 Volumetric Flow meter.

After almost one year of operation it was noticed a malfunctioning of the flow meters. The problem was supposed to be the electro-chemical deposition of vanadium on the inner sensors. The instrument works as stated by the Faraday's law according to which, by applying a magnetic field to a conductive mean there's separation of charges creating an orthogonal electric field. For the electrolytes are two conductive fluids, the instruments apply a vertical magnetic field using two coils on the top and on the bottom of the instrument respectively which separates the charges in the liquid creating an electric field on the horizontal plane. For this reason, two sensors, on the left and on the right, measure the voltage difference between them. As the velocity of the fluid rises the voltage difference grows proportionally so that the flow can be measured being the section of the pipe constant. Even if the instrument was specifically designed for this application, it can be possible that the Vanadium solved in the solutions was affected to electrochemical deposition on the metal surfaces of the lateral sensors creating a non-conductive thin layer and passivating them.

Firstly, it was tried to eliminate the problem by simply washing the pipe with an overnight still bath in a 5 M solution of sulfuric acid, but the results were not satisfying. After this, a pipe cleaner with soft PVC hair was used to try to brush out the possible passivating layer from the sensors. The results this time were more satisfying giving the possibility to restore the measure.

Figure 2.7 shows the working principle of the flow meter as presented on the official E+H website.

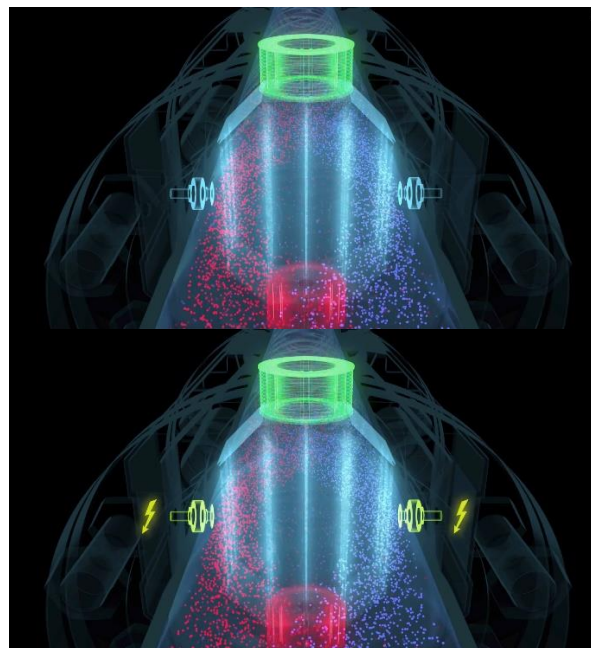


Figure 2.7 Working principle of the E+H flow meter. [14]

- **Differential Pressure:** The plant has two Endress+Hauser Deltabar S PDM75 differential pressure meters connected with a dedicated pressure line between the stack inlet and outlet. They measure the pressure drop for both the catholyte and the anolyte. The system is visible in Figure 2.8. Their output is an analogic current signal (0-20 mA) entering the NI9207 and their supply comes from the measure line.

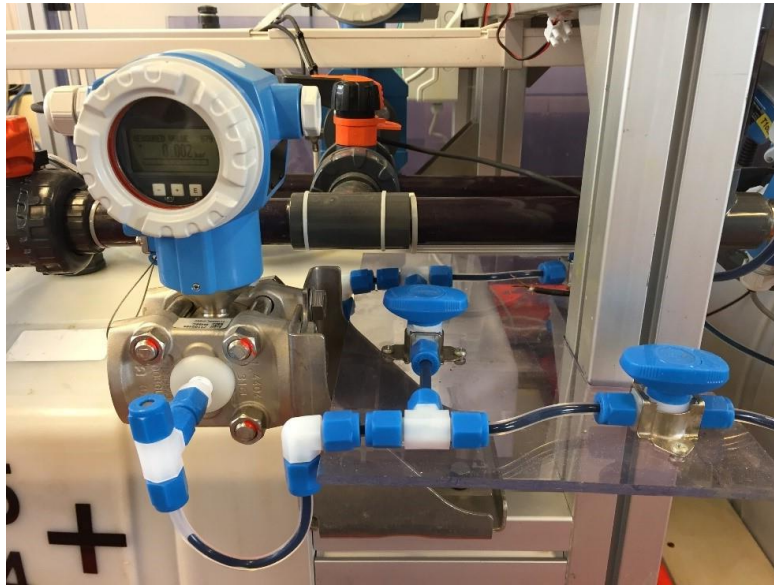


Figure 2.8 Differential Pressure meter with its dedicated pressure line.

- **Thermoresistances:** four thermometers are installed, two for each electrolyte solution, to measure the temperature upstream and downstream of the stack. They are connected to a dedicated module (NI 9216) of the compactDAQ through a four-conductors cable. Two of them are used to measure the resistance, one is to produce the excitation current while the last one is the grounding reference.
- **Wattmeter:** in order to compute the battery efficiency a Seneca Z203 single-phase analyzer is installed which measure the power absorbed by the inverters feeding the two pumps. The instrument has the possibility to transmit as an analogic voltage or current output the voltage, the current or the power passing through the single-phase line. It was employed to communicate to the NI 9207 the active power as a voltage output ranging from 0 to 10 V, where 10 V represents 625 W. Figure 2.9 shows the real object and its schematic connections. It can be noticed that it has its own supply, coming from the left blue cables, while the purple conductors are the ones leading the signal to the

compactDAQ. To be highlighted are the shielded cables connecting the two inverters to the motors in which the shields are connected to the common grounding only in one end.

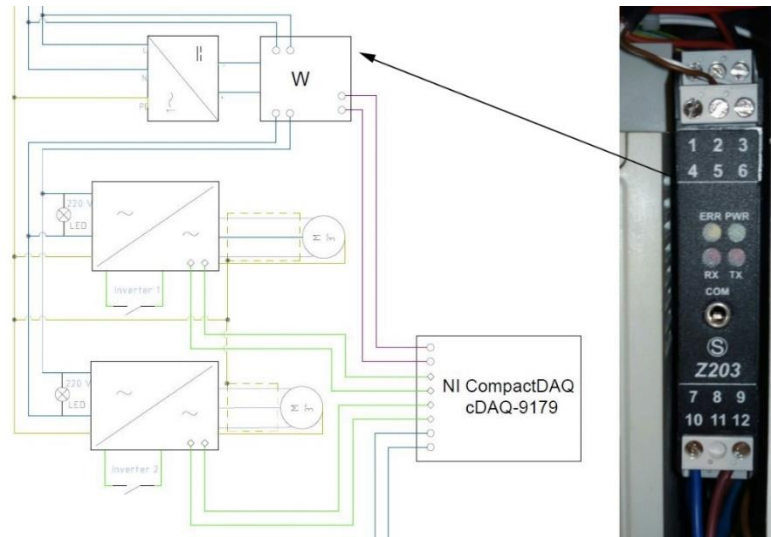


Figure 2.9 Wattmeter and electric connections scheme.

- **Current Transducer:** a LEM HASS 50 S was initially used to measure the current flowing inside or outside the stack but it was then replaced with a LEM HASS 200 S because of its wider range of measure considering it could have been possible to reach higher currents than the stated ones in the discharge mode. The transducer transforms the current flowing in an analogic voltage signal and sends it to the NI 9207 module.

2.2.2 Electric Power and Measurement Circuits

Schemes of the wiring connections were made using AutoCAD Electric, a dedicated software for drawing electrical circuits. Figure 2.11 represents the connection among the devices dedicated to the measures. On the left the equipotential grounding bar is shown. The PLC and the CompactDAQ with all its modules are shown in detail. Figure 2.10 shows the specific connections inside one of the modules of the CompactDAQ acquisition hardware, comprehensive of the colors of the cables and the number of pins. Figure 2.12 is dedicated to the power connection including LEDs, lights, switches, relays and motors. In the two general schemes the cables are distinguished by their colors:

- Blue: power connections for both alternate or continue currents
- Purple: measure connections for both digital or analogic signals coming from the sensors or the measurement devices
- Green: control connections for all the wirings through which a current or voltage control is made

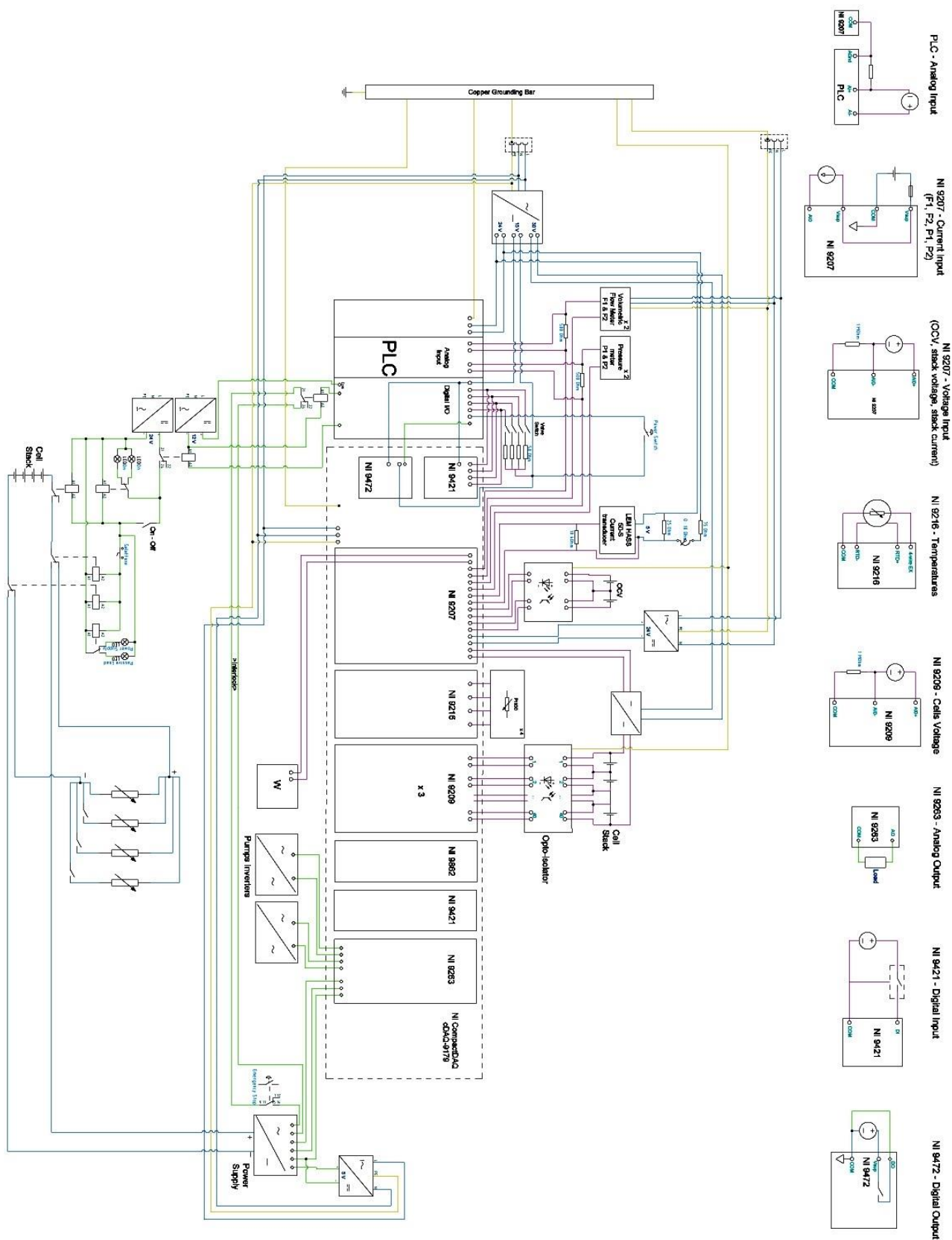


Figure 2.11 Electric connection of the measurement system. Electric schemes of the NI modules are drawn.

2.2.3 Security devices and measures

To ensure a major and intrinsic safety to the whole plant it has been decided to install a PLC and some other devices like microswitches and emergency buttons.

A Elsynt Slim Line PLC (Programmable Logic Controller) was installed to prevent problems deriving from a malfunctioning of the LabVIEW software. Once programmed this device works independently from the computer. It is composed by three modules, the first has the programmable board and it can be connected via USB to a computer, the second acquires the analogic signals and the last one is a digital Input/output interface.

The PLC receives the supply from a 24 V source (blue cables entering the first module) and it's grounded. It takes as an analogic input the voltage signal from the two volumetric flow meters and the two differential pressure meters. It has five digital inputs that are four valves in the piping system and a manual mushroom push button called *Power Switch*. It has two digital output both connected to a relay. The first commands the interlock of the power supply. If the flow measured it's not enough the PLC stops the consent and the power supply is switched off. The second's connected to a 12 V relay which in turns commands the 24 V excitation circuit of a Zhejiang Aokai Electric ASW400 DC Magnetic Contactor. Its purpose is to open the circuit between the stack and the power supply. If a LabVIEW Boolean switch is turned off or the manual *Power Switch* is pushed the circuit opens. Figure 2.13 shows the regulations described above.

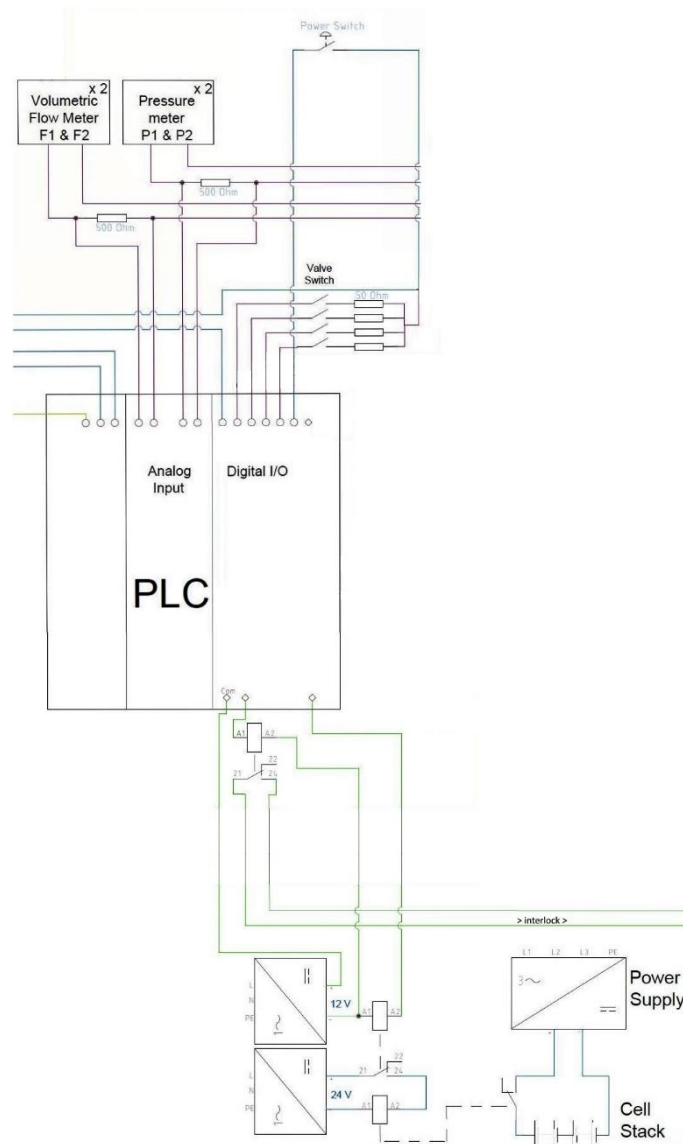


Figure 2.13 PLC connections.

Moreover, to avoid the plant to be put in operation if not all the valves are in the correct position two more microswitches have been mounted on the two valves downstream of the stack. These microswitches command two relays on a series connection with the emergency stop. If only one of the three opens, two 230 V AC relay's coils are not excited anymore and so one opens the supply to the whole plant while the other interrupts the interlock of the Power Supply. Figure 2.14 shows the connection of this part of the power circuit.

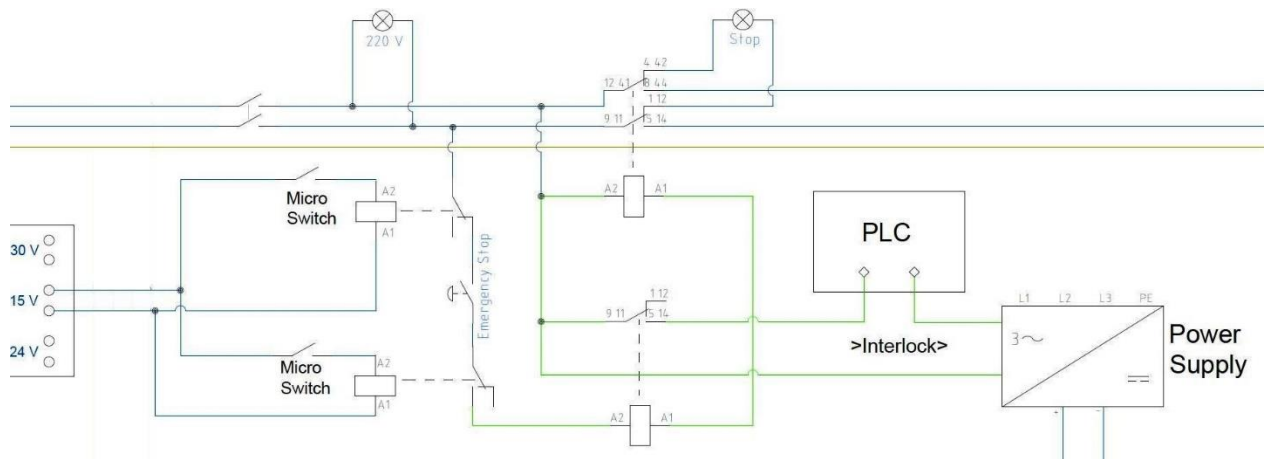


Figure 2.14 Micro-switch security system.

2.3 Electromagnetic interference protection

One of the main problems during the measurement activities was represented by the consistent presence of disturbance interference. In particular voltage and current, which are fundamental for the experimental control of the battery, were mainly affected by this issue.

The problem was pinpointed in the presence of the PWM (Pulse-width modulation) inverters which command the pumps. These devices create both a conducted disturbance on the line and a radiated disturbance on the surrounding environment.

To try to eliminate the problem many operations were made on the electrical plant. Firstly, two filtered power entry modules have been installed one upstream of the inverters' power supply to limit the spreading of conducted disturbances in the grid and one upstream of the CompactDAQ to limit the incoming interferences, but no significant results have been reported. Secondly, two parallel capacitors (1 μF and 100 nF respectively) have been installed upstream of the LEM transducer to work as physical filters, but, again, no noteworthy results were reported. Moreover, the signal and power cables going from the LEM to the CompactDAQ were substituted with shielded cables and the results were not sufficiently good. Lastly, as suggested in the EMC (Electro Magnetic Compatibility) regulation and reported in [15], the non-shielded cables connecting the pumps with the inverters have been substituted with specific inverter-motor cables. Their peculiarity is to separate the grounding cable to the tripolar ones which are shielded as shown in Figure 2.15. In this way even if some interference travels in the grounding cable it can't propagate to the power cables.

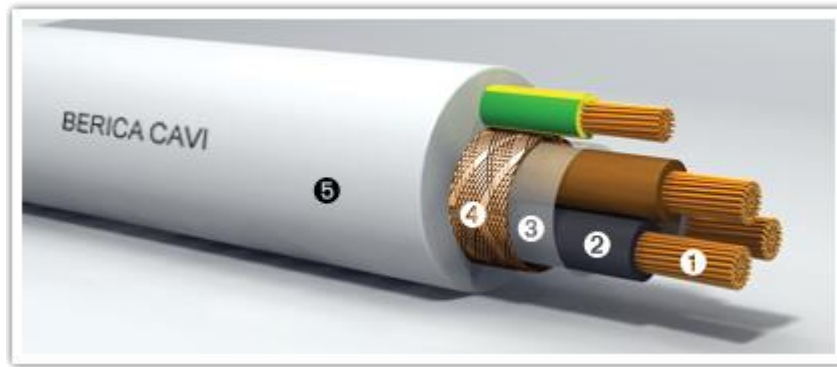


Figure 2.15 Inverter-motor cable section. Courtesy of [16].

The results agreed with what was expected keeping the measures in an accepted range of errors. To strengthen the effect of a copper shield, the power cables have been inserted in additional external copper pipes.



Figure 2.16 Copper shielding pipes for motor-inverter cables.

As the inverters are a source of radiated electromagnetic fields it was decided the construction of a shield. A shield is typically a metallic barrier to radiated magnetic fields used for both reducing emissions from an electrical equipment and increasing immunity of a device [17].

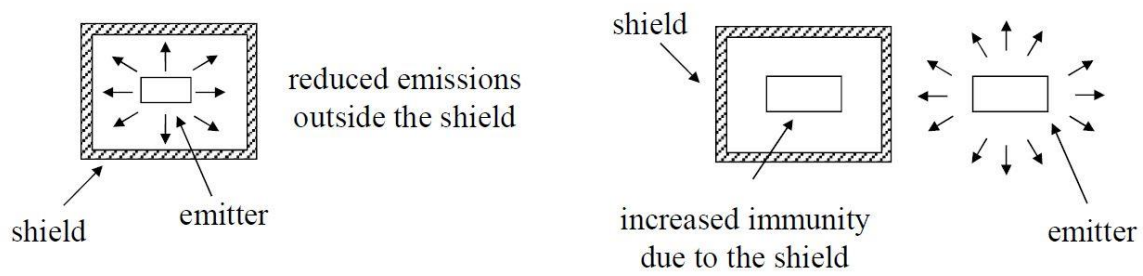


Figure 2.17 Electromagnetic shields examples. [17].

The shielding effectiveness, defined as twenty times the logarithm of the ratio between the incident and the transmitted electric (or magnetic) field, is a positive number that represents the reduction of the magnitude of the phasor of the electric (or the magnetic) field when subjected to a metallic shield. It is the sum of three terms: absorption loss A_{dB} , reflection losses R_{dB} and multiple reflection losses M_{dB} .

Absorption loss is a function of the thickness of the metal shield and the product of its conductivity and permeability. It increases with increasing frequency as \sqrt{f} , on a logarithmic scale. Reflection loss is a function of the ration between conductivity and permeability and varies with the frequency at a rate of -10 dB/decade. It doesn't depend on the thickness of the shield. Multiple reflection losses can be neglected in the case of a thick shield [17].

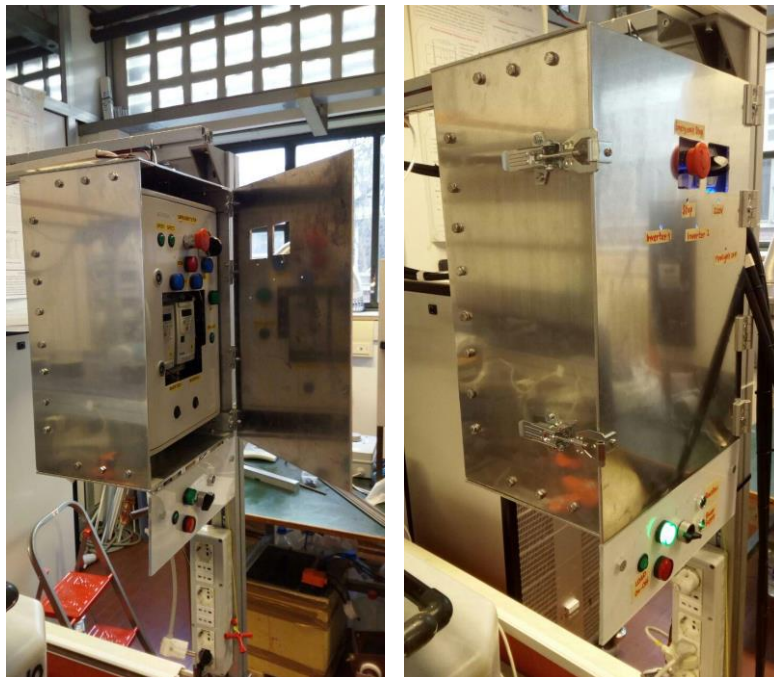


Figure 2.18 Shielding metal box.

Figure 2.18 shows the metal box made to enclose the two inverters and the electric panel with all its components.

Before these alterations the mean current value when only the inverters were fed but no current was given to the pumps, was in the order of 0,3 A instead of the expected null value. When then the pumps received a 50 Hz feeding the disturb was growing of another 0,5 A, for a total of 0,8 – 1 A. After the installations of these protection devices the interferences have almost completely been eliminated.

2.4 LabVIEW acquisition system

LabVIEW (Laboratory Virtual Instrumentation Engineering Workbench) it's a National Instruments graphic programming code [18]. Its peculiarity which makes it a user-friendly interface, is represented by the Visual Instrument (VI) made by the Front Panel, the Block Diagram and by an icon representing it [19]. In the Front Panel the user can find the controls to be used to give inputs to the program, the indicators to visualize the results and any other interactive tool. The Block Diagram instead is where the real code is. Here, all the icons representing inputs, outputs and functions can be wired and arranged to create the main structure of the program. LabVIEW, as said, works with VIs which are the counterparts of functions or subroutines in codes like C or BASIC [19]. So, a VI can contain subVIs inside the main program.

When this thesis work started the program was already defined in its main structure and complete in lots of its parts but still in a raw condition. The work relative to LabVIEW was focused on the development of subroutines of the state machine for specific operations and on the creation of SubVIs to group some procedures and simplify the viewer understanding of the program. These works will be explained in detail in §2.5, §3.2 and §4.1.

In the following chapters it will be briefly introduced and described the structure of the program developed for the control of the VRFB-IS Experiment. For a more detailed description the reader can refer to [20].

2.4.1 LabVIEW Block Diagram

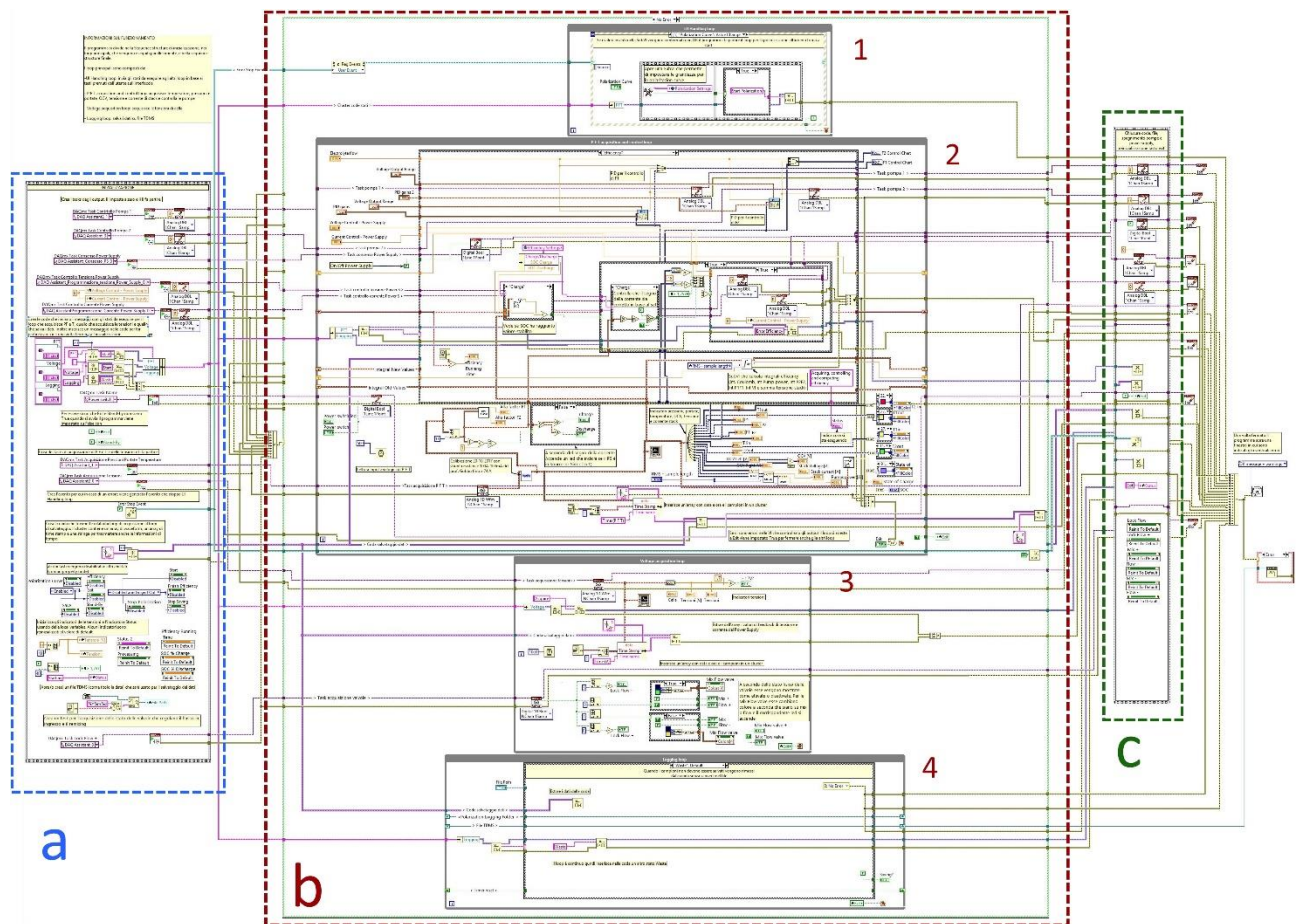


Figure 2.19 LabVIEW interface Block Diagram. a) Initialization, b) Error Case Structure (Program's main core), c) Final Sequence

Figure 2.19 shows the block diagram of the program. It's subdivided into three main sectors: a, b and c.

- a) *Initialization.* In this section the program begins with some preliminary operations for the start-up of the routines and to link with all the connected devices e.g. the CompactDAQ chassis. Besides from initializing all the *tasks* of the NI modules, the program creates the FIFO queues that will govern the state machines (as described later), resets some values from previous utilizations of the program and generates a folder path inside the working folder named as "yyyymmdd" of the current day. Since this section is all confined inside a *Time Structure*, before sending the generated signals to the following operations, all the ongoing processes must be concluded. All the errors lines coming out the VI's blocks are merged in a single cable which govern the following *Error Case Structure*.

b) *Error Case Structure*. This case structure contains all the operations enclosed in *b* (e.g. b1, b2, b3, b4) and works as follows. If one or more errors are coming from the error line, the case structure switches to the “*Error*” case which does nothing except connecting the wires as they come from the *Initialization* to the right end of the case and brings all the signals to the final sequence. If no errors are present, the “*No Error*” case happens, and the program can work properly. Inside this case structure four sub-structures can be found: the while loop called *UI Handling Loop*, the *P F T Acquisition and control loop* state machine, the while loop named *Voltage Acquisition Loop* and the *Logging Loop* state machine. The decision of diving the main program in parallel sub-structures was taken firstly to have the possibility of doing different and independent operations separately and secondly to select the velocity of each process by deciding if the High-Speed Mode or the High-Resolution Mode would have been the best choice.

b1) *UI Handling Loop*. It’s composed by an event case inside a while loop. This User Interface while loop is used to modify the execution sequence of the state machines consequently to the pressure of buttons on the Front Panel. Quite in all the cases (except some described later) a string is written in a queue and is given as an output of this event case that so will govern the corresponding state machine by entering its case selector pin. The event case inside the while loop stays inactive and waits for the user to produce an event in order to avoid the polling. This happens when the program continuously checks a specific event to happen and ignores the others. Some special events are included like the sudden arrest of the P F T while loop to which the stop of the program follows, or the pushing of the LabVIEW window close button which produce a warning message that make the user choose if confirming the exit from the program or the elimination of the action.

b2) *P F T Acquisition and control loop*. With this state machine it’s possible to control the electrolytes flows, the current and voltage parameters during charge and discharge, the temperatures and the pressure. Most of acquisitions are performed continuously no matter the case the state machine is carrying out so that the user can keep under control the state of the plant while doing other operations. The queue called “P F T” is the one governing the state machine enclosed inside the while loop. The state machine presents lots of cases, but they are linked in four main routines designed to follow a predefined flowchart.

- *Start and Acquisition (Default)*: In this routine the program pass through a sequence of reset and restart for some parameters and then passes to the Default case. In this state, LabVIEW acquires all the data coming from the test facility and simply regulates the pumps through the inverters commanded by a PID and keep trace of it on the graphs of voltages, temperatures and flows. The

case stops if the user pushes the button Stop on the front panel. If the flow lowers below a limit imposed by the alfa-factor or if the voltage of one of the cells gets higher than 1,7 V the power supply cannot work and it's deactivated. In any moment the user can decide if saving or starting any of the following procedures simply by clicking the corresponding button.

- *Temperature Control*: at the moment the temperature control routine starts every time the user put the plant in Stand-by. In this eventuality the pumps stop pumping the electrolytes into the stack so that the reagents that are still inside start rising their temperature due to self-discharge reactions. The main cause of this effect is the vanadium ions crossover through the membrane, as a matter of facts the diffusion reactions of all the four ions species used in the VRFB are exothermic so that the heat produced is important [21]. The crossover lasts until the concentration of the two ions in the catholyte and in the anolyte reach the same level so a loss in capacity and SOC happens. But if the capacity loss can be easily restored by periodic remixing of solutions as suggested in [21] the losses due to precipitation of V(V) at high temperature is way more complicated even if not irreversible. This aspect will be described better in chapter §5. So, the purpose of this routine, composed by several cases, is to ensure periodical recirculation of the electrolytes not to reach dangerous temperatures. At the beginning it registers the start time and waits for two events to happen to restart the pumps for a 30 s long recirculation. The first one happens when the time set by the user in the Stand by Time indicator in the front panel elapses. On the other hand, if one of the temperature overcome 33°C. After the 30 seconds passed, the time is registered again until the stand-by mode is concluded by the user. This method is effective but not to waste too much SOC for long periods of stand-by due to the self-discharge a better algorithm is in development basing on the study reported in §5.

- The *Polarization Curve* and *Efficiency* routines were developed in this thesis work and are widely described in chapter §3 and §4 respectively.

b3) *Voltage Acquisition Loop*. This loop is dedicated to the acquisition of the single cells' voltages from the NI 9209 modules. The values are plotted in the second front panel's graph and read by the indicators of section 9 of Figure 2.20 which give information about the state of each cell. Moreover, this loop controls the valves' microswitches and their status.

b4) *Logging Loop*. This state machine is devoted to save data into TDMS files when required by the user. The TDMS file is a binary file specifically created to interface with National Instruments products [22]. It's totally compatible with Excel but its dimensions on the disk are reduced and its streaming on disk. This

state machine contains 4 possible routines: one for the manual Saving, one for the Timed Saving, one regarding data coming from the Polarization routine and the last for the Efficiency routine data. The first two cases are activated from a user's action while the others come automatically at the end of each process.

- c) *Final Sequence*. In this sequence all the queues are emptied, all the analogic control outputs are set to zero and the status bar shows the user "Exit". After this, all the tasks are eliminated, and all the error wires connected and sent to a VI that shows the eventual error message before the program stops.

2.4.2 LabVIEW Front Panel

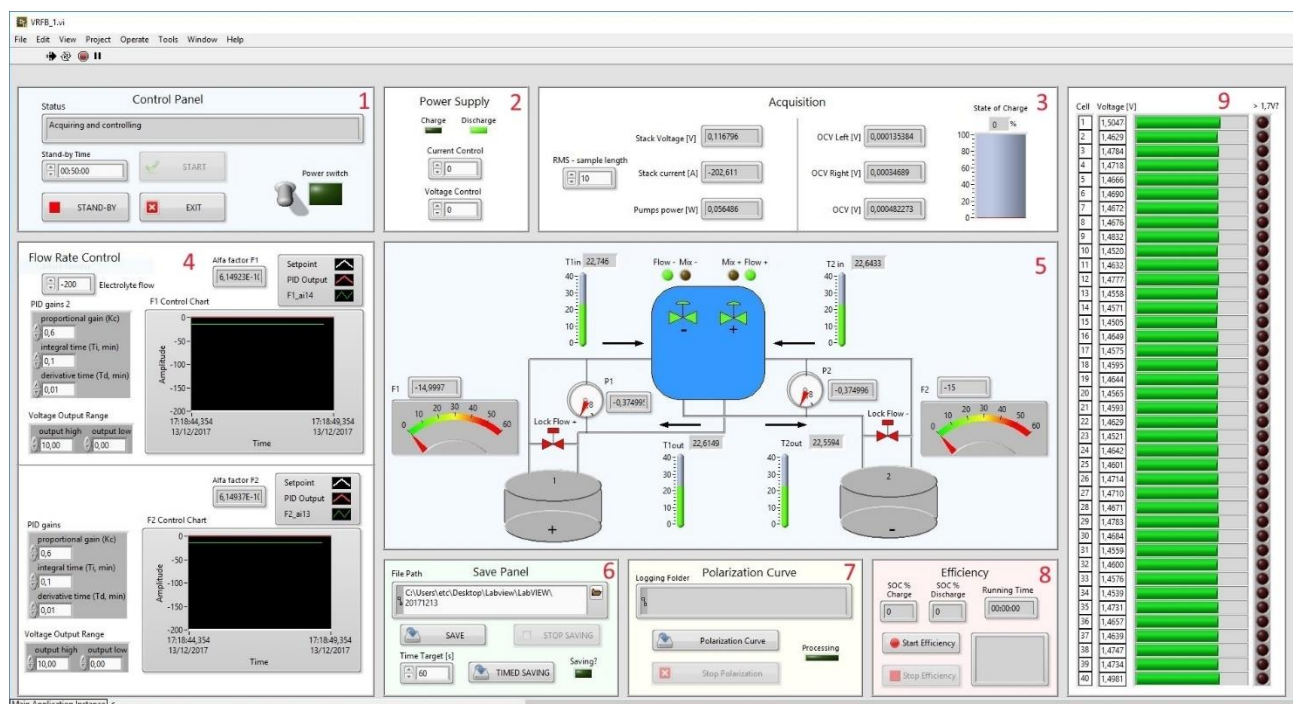


Figure 2.20 LabVIEW interface Front Panel.

The Front Panel is what the user uses to dialogue with the program and it's where all the visual properties of LabVIEW show their importance. The panel is divided into sections for a better clarification and to create an easy-to-use interface for new users.

Figure 2.20 displays the front panel that will be briefly described in the following.

1. **Control Panel.** The *Status* bar is an indicator where the code writes what the program is doing. Each case is linked to an output message describing the occurring operation. The *Start* and *Exit* buttons allow the user to start or stop the program respectively in each

moment. If the *Stand-By* button is activated, the program switches to the temperature control case where the pumps are deactivated and turned on to make the electrolytes recirculate just if the temperature rises above a preset temperature or if a certain amount of time is elapsed. The *Stand-by Time* control sets the time the program would wait when in Stand-by mode. The *Power Switch* toggle and LED are what gives the program the consent to activate the power supply as described in §2.2.3. If the toggle is activated the LED turns on.

2. **Power Supply.** Two LEDs *Charge* and *Discharge* turns on when the battery is charging or discharging respectively. They are based on the current sign so that, if it's positive the system is charging and vice versa. Since the current transducer is floating around zero, when no current is given or required to the system, the LEDs switch on only if the registered absolute value overcomes 1 A. The *Current Control* and *Voltage Control* controls can be set to dialogue with the Power Supply and impose a certain value of current and voltage correspondingly when it is in remote operation mode, or show the present values when in local mode.
3. **Acquisition.** The left side of this structure is dedicated to *Stack Voltage*, *Stack Current* and *Pumps Power* coming from the respective measure devices. The *RMS – sample length* control can be set to stabilize the measured values by computing the RMS with the imposed number of samples. On the right side the left, right and total OCV are shown coming from the OCV cell on the frontal part of the stack and a *State of Charge* tank indicator is present. Through the algorithm described in §2.5.2 the tank fills and express the % SOC basing on the measured OCV. It's an important visual tool because by filling and changing color this tank gives the user an immediate impression on the state of charge without consult tables of conversion from OCV to SOC.
4. **Flow Rate Control.** This section has two symmetric parts on the top and on the bottom which are related to the PID flow rate control of the anolyte and catholyte: *PID gains* gives the proportional, integral and differential constants, *Voltage Output Range* sets the max and min voltages, *F1 and F2 Control Charts* visually show the setpoint, the PID output and the signal from the flow meters, on the top *Electrolyte flow* is what sets the goal of the PIDs. The *Alfa Factors*, computed as in §2.5.4, indicates the ration between the given and the stoichiometric required flow.
5. **Plant Scheme.** In this section there's a basic representation of the plant including valves, tanks, pipes and the indicators related to the measure devices. In particular four color changing thermometers indicate the temperatures, two gauge-manometers show the pressure drop and two meters indicator for the flows.
6. **Save Panel.** In the save panel section all the options for saving are present. The *File Path* indicates the folder path including the file name where the data will be saved. By pushing the *Save* button the program will start saving the acquired data and it'll stop

only when the *Stop Saving* button is pressed. Alternatively, to save for a predetermined amount of time, the user must set this interval in seconds in the *Time Target [s]* control and push *Timed Saving*. The program will automatically save just for the desired amount of time. In any case if the program is registering any data onto a file, the *Saving?* LED turns on.

7. **Polarization Curve.** This section is dedicated to the part of program expressly developed to acquire data useful to compute and plot the polarization curves. The description of the front panel and the connected routine in the Block Diagram is in §3.2.
8. **Efficiency.** This section is dedicated to the part of program devoted to compute the efficiencies of the whole plant. The description of the front panel and the connected routine in the Block Diagram can be found in §4.1.
9. **Cell Voltage Indicators.** This section is dedicated to the state of the single cells. The first column indicates its number (from 1 to 40), the second is the numeric value of the voltage at its ends, the third is a filling bar indicator showing visually the number in the second column and in the last one a LED turns on if a cell voltage overcome 1,7 V. In this case the program stops the power supply immediately to ensure the safety of the cells.

Moreover, in the Front Panel interface there are two graphs, not shown in Figure 2.20, that display explicitly some of the acquired data as a function of time. The first one is dedicated to flows and temperatures while in the second all the 40 stack voltages are plotted.

2.5 LabVIEW Ancillaries

An important part of the work was focused on the simplification of the already written code in the block diagram with the introduction of SubVIs. This was majorly made to simplify the user in the understanding of the general scheme. In the following paragraphs the SubVIs are reported with their scheme and some specifications about their principles.

In Figure 2.21 it's presented an example of the clarification visual impact that follows the introduction of subVIs in the block diagram.

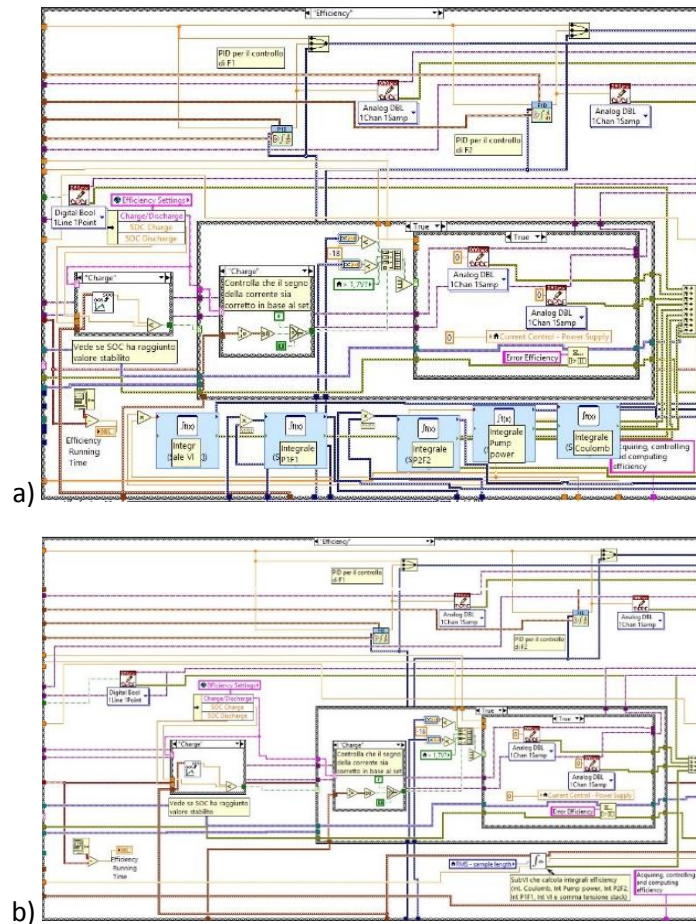


Figure 2.21 An example of how the adoption of SubVI can clarify the view in the block diagram.
The block diagram in the case “Efficiency” before a) and after b) the use of a SubVI.

The presented SubVIs are: LEM Current Transducer Calibration SubVI, OCV to SOC SubVI, Integral Efficiency SubVI, α -factor SubVI. The Polarization and Efficiency SubVIs will be described later respectively in §3.2 and §4.1.

2.5.1 LEM Current Transducer Calibration SubVI



Figure 2.22 LEM current transducer SubVI logo.

It was noticed that the transducer employed to measure the current absorbed or produced by the stack was affected by an error. In order to correct its value and get a more precise and stable measure, a calibration was achieved using a shunt resistor.

The calibration was performed as follow. First of all, the shunt calibrated resistor was connected to one of the two conductor which link the power supply and the cells stack. The shunt resistor is standardized to give 99,51 mV if 100 A flows through it. The current flowing through the resistor was measured through a multimeter and on the computer's screen it was read the current from the LEM current transducer to be calibrated. The current was risen from 0 to 74 A with a 2 A step size basing on the declared current given by the power supply indicator.

Afterwards, the difference between the current registered by the LEM and the one measured at the end of the shunt resistor was plotted as a function of the LEM current as shown in Figure 2.23.

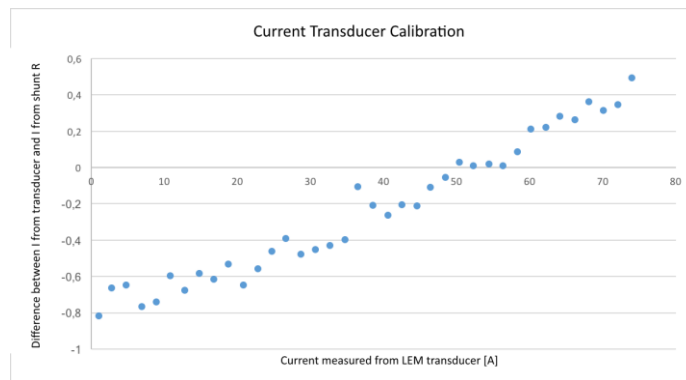


Figure 2.23 Graph for the calibration of the LEM current transducer. It plots the difference between the current from the transducer and the one from the shunt resistor as a function of the current from the transducer.

Lastly, a polynomial second order interpolation of this curve was figured, and it was used to build the SubVI.

$$y = x + (0,0001x^2 + 0,0096x - 0,7785) \quad (7)$$

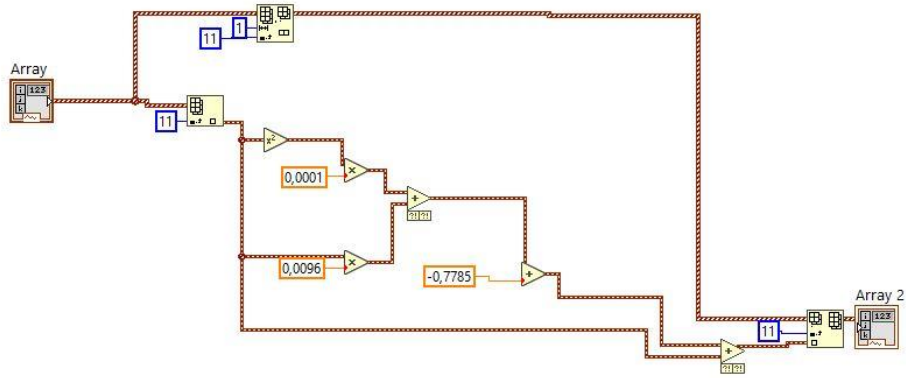


Figure 2.24 LEM calibration SubVI structure

As it is shown in Figure 2.24 the current signal is extracted from the acquisition array coming from the NI-DAQ and equation (7) is applied to correct and stabilize its value. Finally, the new value of current is replaced in the initial array which is given as an output.

2.5.2 OCV to SOC SubVI



Figure 2.25 OCV to SOC SubVI logo

As it's widely described in the literature [1], [5] and [9], there is a connection between OCV and SOC in a VRFB system. The relation comes from Nernst equation and it's stated by expression (8),

$$E_{OCV} = E_{OCV}^0 + \frac{2RT}{nF} \ln \frac{SOC/100}{1 - SOC/100} \quad (8)$$

or by the reverse formula (9).

$$SOC = \frac{e^{\frac{nF}{2RT}(E_{OCV} - E_{OCV}^0)}}{1 + e^{\frac{nF}{2RT}(E_{OCV} - E_{OCV}^0)}} * 100 \quad (9)$$

Where

- SOC is the State of Charge expressed in %
- E_{OCV} is the Open Circuit Voltage of the stack
- E^0_{OCV} is the Open Circuit Voltage at a State of Charge of 50%. Its value floats generally between 1,3 to 1,4 V. The selected value is 1,37 V.
- T is the Temperature in K
- n is the numbers of moles of electrons involved in the reaction, which in this case it's 1.
- R is the gas constant (8,314472 [J/K mol])
- F is the Faraday constant (96485.3365 [C/mol])

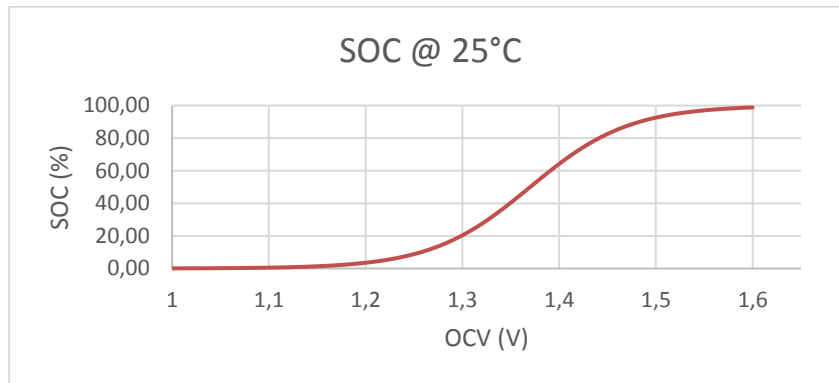


Figure 2.26 State of Charge % as a function of the Open Circuit Voltage computed with the theoretical formula at 25 °C.

The graph in Figure 2.26 is the graphical representation of the inverse formula (9) for an average temperature of 25°C that was chosen as reference. Since this equation is a function of temperature, it was decided to implement the SubVI using the average of the four temperatures of the electrolytes entering and going out the stack that are an input data for the program.

In the implemented SubVI (Figure 2.27), the temperatures and the left and right OCVs are extracted from the input array. The mean of the temperatures is computed and the total OCV (sum of the two half cells OCVs) are used to compute the SOC %. This is given as a numeric output of the SubVI.

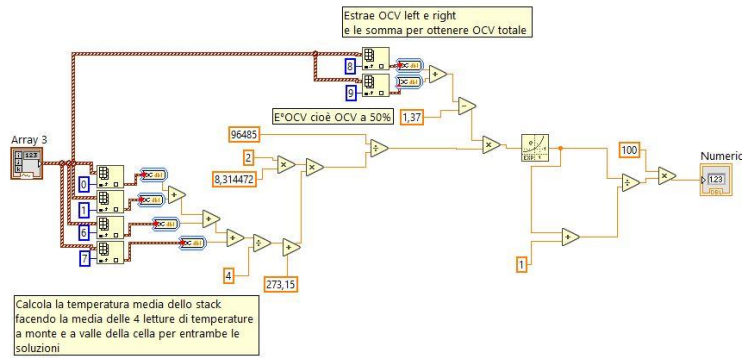


Figure 2.27 Block Diagram of the routine to convert OCV into SOC.

The SubVI is present in many parts of the program (e.g. *Efficiency* routine, see §4.1 LabVIEW Automation) confirming the importance of adding compact SubVIs for a clear program structure. In particular, this SubVI is used to control a color changing tank indicator on the Front Panel that gives an immediate evidence of the State of Charge of the battery as shown in Figure 2.28.

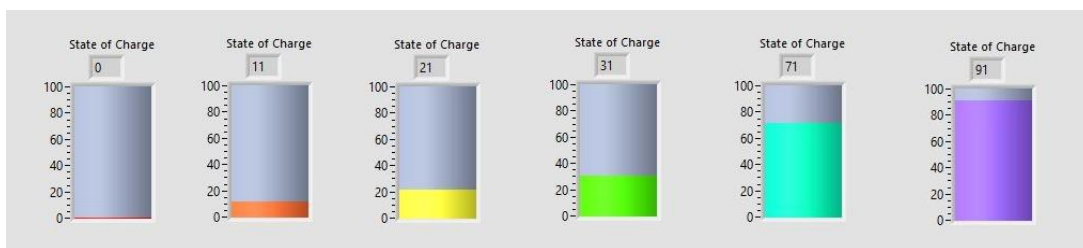


Figure 2.28 State of Charge tank indicator in the front panel.

2.5.3 Integral Efficiency SubVI



Figure 2.29 Integral Efficiency SubVI logo.

This SubVI it's the core of the *Efficiency* routine that will be described later (§4 Efficiency). In this SubVI five integrals and the total stack voltage are computed and sent as an output to the program inside an array. The integrals are presented in Table 2.2

Coulomb	$\int I dt$	(10)
Pump Power	$\int P_{pumps} dt$	(11)
P2F2	$\int P_2 F_2 dt$	(12)
P1F1	$\int P_1 F_1 dt$	(13)
VI	$\int VI dt$	(14)

Table 2.2 Integrals of the Integral Efficiency SubVI.

Where

- I is the stack current,
- V is the stack voltage,
- P₁ and P₂ are the anolyte and catholyte pressure difference between inlet and outlet,
- F₁ and F₂ are the anolyte and catholyte flow,
- P_{pumps} is the power absorbed by the pumps and the inverters acquired from the wattmeter.

The *Stack volt in* numeric control (Figure 2.30) represents the data of the stack voltage summation coming from the previous iteration to which the new value of Stack voltage is added from the acquisition array. It's then saved in *Stack volt out* which it's finally saved in the shift register ready to be used in the following iteration. At the end of the *Efficiency* procedure this value will be divided for the total number of samples to achieve the mean stack voltage during the charge or discharge process.

How the other values will be elaborated it'll be described later in the already mentioned chapter §4 (page 59).

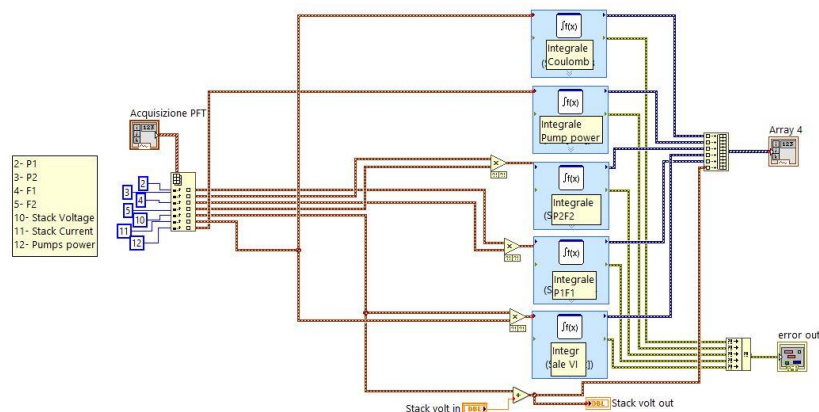


Figure 2.30 Block Diagram of the integral efficiency SubVI

2.5.4 α -factor SubVI



Figure 2.31 α -factor SubVI logo.

The α -factor is a very important parameter for the plant control. It indicates the ratio between the given flow and the stoichiometric necessary one. It is computed in two different ways depending if the system is charging or discharging (Equations (15) and (16) respectively).

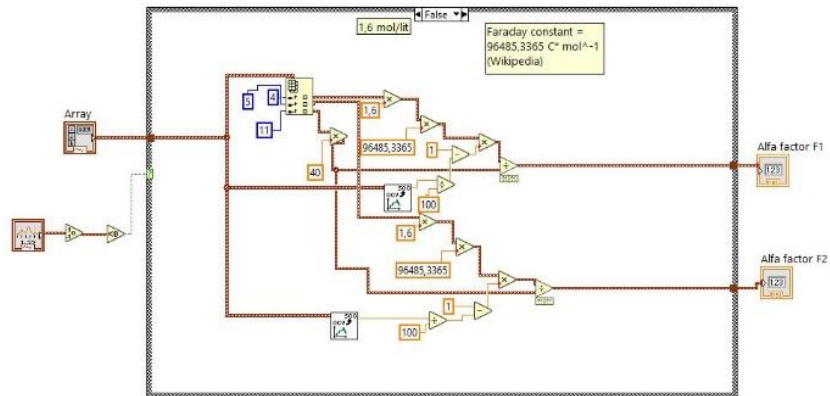
$$\text{Charge} \quad \alpha_c = \frac{Q C_V F(1 - SOC)}{40 I} \quad (15)$$

$$\text{Discharge} \quad \alpha_d = \frac{Q C_V F(SOC)}{40 I} \quad (16)$$

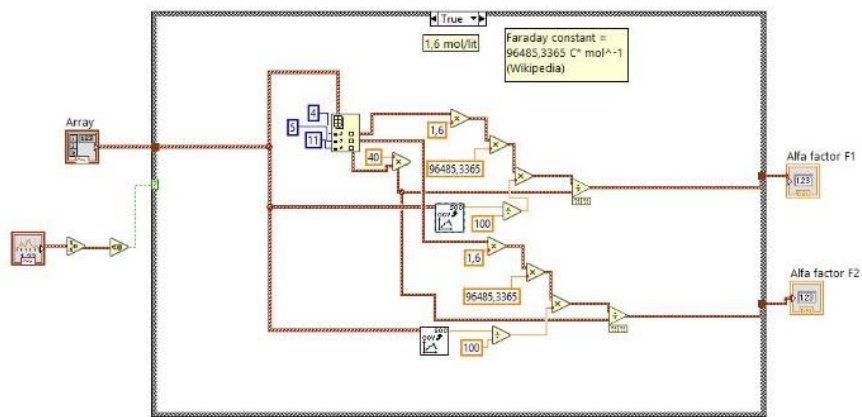
Where

- Q is the flow
- C_V is the molar concentration of Vanadium
- F is the Faraday constant
- SOC is the state of charge expressed in %
- I is the current.

Using this parameter, it can be possible to regulate the flow to maintain a certain overfeeding of the plant not to risk some part to be damaged. As a matter of fact, if the electrolyte in a cell is not enough (even locally) the potential is directly applied to the cell components with the risk of serious injuries. In general, a value over 8 is suggested to prevent any dangerous situation. The stack must be overfed because it must be ensured a minimum quantity of reagents to reach its active sites. Transport losses due to the wettability and mass transport velocity inside the porous electrode makes this value rise and consequently the overall efficiency lowers because more energy is required to feed the electrodes. This SubVI simply computes the two alfa factors for the two electrolytes in the case of charge or discharge depending on the current sign.



a)



b)

Figure 2.32 The two cases of the alfa-factor SubVI. a) in case of Charge refers to equation (15), b) in case of Discharge uses equation (16).

3 Polarization Curves

A polarization curve is a plot of current density versus electrode potential for a specific electrode-electrolyte combination. In the study case, the polarization curves display the stack voltage output of the battery for a given current density load. It is characterized by a peculiar “s” shape presenting a fast decreasing of voltage for low and for high current densities. It can be divided into three zones: Activation losses, Ohmic losses and Concentration losses.

When the current density is zero, the Open Circuit Voltage (OCV) of the stack is measured and, as it was previously said, it gives information about the SOC.

In the activation zone, for low current densities, the losses are mostly caused by activation and electronic transfer overpotentials, due to the reactions taking place at the electrodes. Every chemical reaction needs some overpotential to activate the site and make the reactants turn into products. In this zone there is a drastic fall of voltage.

The ohmic zone is a long linear part of the curve where losses are mostly imputable to resistances in electronic and ohmic conductors i.e. current collectors, electrodes and membranes.

Finally, for high values of current density the voltage falls rapidly because the reactants are consumed at a too fast rate or because products remain in the active sites for too long. This zone is easily recognizable by the presence of a knee. Figure 3.1. shows an example of polarization curve.

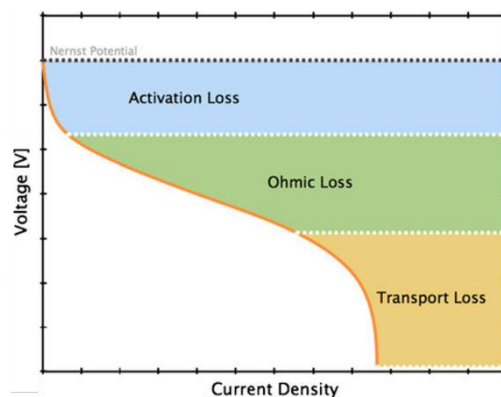


Figure 3.1 A general polarization curve.

In our case, the fixed current is given by a power supply specifically designed to be settable in remote by the LabVIEW interface. Its specifics permit to use it both as a sink or as a source of

energy giving the possibility to plot polarization curves in the case of charging or discharging the battery. For every specific SOC and Flow values combination, the current steps up from zero to a set max limit. The power supply can reach a maximum of 75 A so that, to reach higher values of current a variable resistor (Figure 3.2.) was initially used. Since its behavior is passive it was used only in the discharge case. When the variable resistance was in operation manual data collection was done.

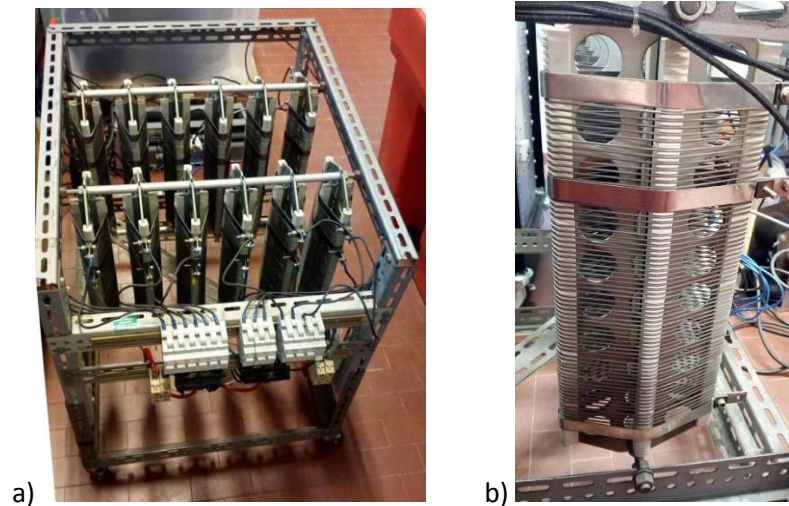


Figure 3.2 a) The firstly used variable resistor as a parallel of 12 variable resistors. The switches and the cursors permit the regulation of different configuration to reach the desired value of resistance. Its value depends by the configuration and connection adopted. $R=15\ \Omega$ for each resistor. b) Detail of the cursor.

Some preliminary data, collected by a first campaign, showed us that the declared limits of the test facility were underestimated. In order to experimentally estimate them, a second campaign of study has been programmed. All the results are shown in chapter §3.3. Apart from the Voltage, which limit is imposed by the electrochemical behavior of the materials, the current was limited by the stack constructor to a max of 72 A and consequently the maximum rated power was set around 3,6 kW.

3.1 Passive load construction and cabling

To collect the necessary data for the second data collection campaign, a specifically designed passive load was built, and an adequate circuit was designed to allow the user to simply switch from one load to the other to make the data collection manual.

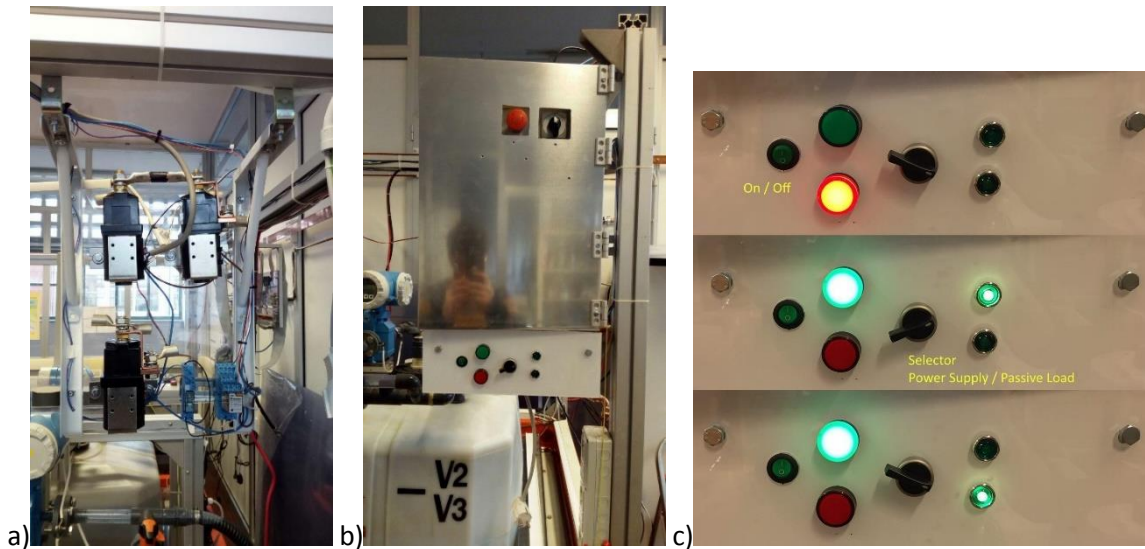


Figure 3.3 a) Contactors panel and cabling, b) front panel complete of switches and LEDs for load switching, c) details of the user selector panel in operation.

As first step, the previously used contactor was replaced with one capable to interrupt higher currents. Then, a circuit was designed to allow the user to choose the load between the power supply and the passive load. As it can be seen in Figure 3.4 the stack is connected to the load only if two switches are both short-circuited. The first one is a telematic consent coming from the PLC and the LabVIEW program, the second is a manual switch marked with “On/Off” that can be found in the user panel below the electric panel outside the metal shield. Once both these switches are activated, the red LED turns off, the green LED turns on and the monopolar contactor’s coil is excited to allow conduction. Two more bipolar contactors, one for the + cable and one for the – cable, can switch the current to the power supply or the passive load. The user can choose which one to supply by simply turning the switch in the front panel. To signal the user which one is currently in operation, the corresponding LED turns on in the panel. The electrical scheme is shown in Figure 3.4, while Figure 3.3 shows the user interface panel and the contactors.

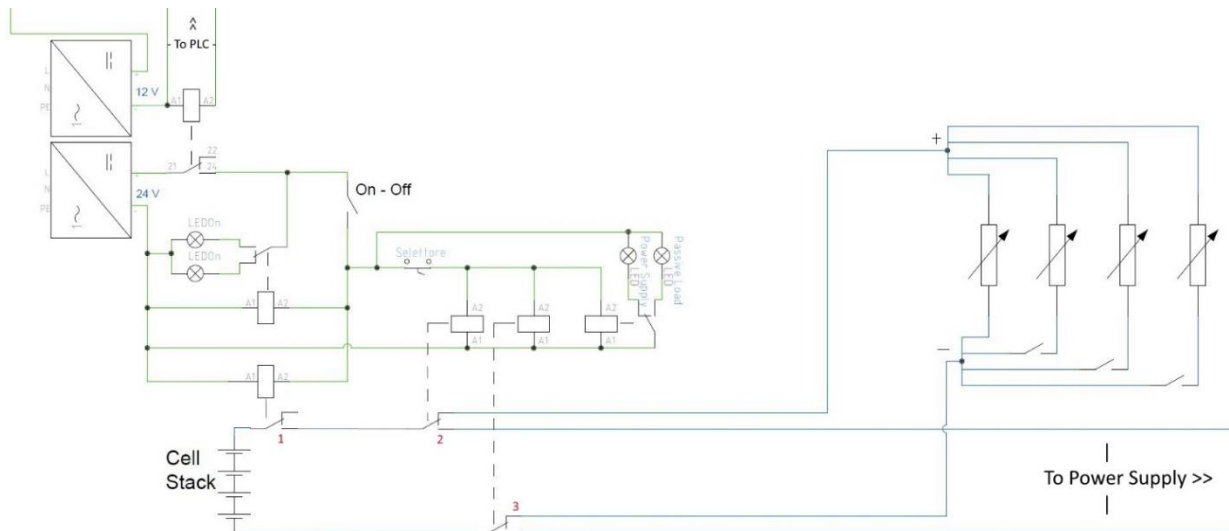


Figure 3.4 Electrical scheme of the load selector. Green cables are the control cables while blue cables are the power cables. 1 is the bipolar contactor to allow conduction, 2 and 3 are the tripolar contactors that switches from the passive load to the power supply.



Figure 3.5 Passive load. Four variable resistors composing the load. On the right a particular of the slider to adjust the resistance.

The passive load is composed by four variable resistor each with the characteristics listed in Table 3.1. Via manual switches the resistance of the whole load can be adjusted and so the dissipated power. The whole passive load is shown in Figure 3.5 where all its components are pointed.

Resistance range	0 – 1.0 Ω
Current	100 A
Power	10 kW

Table 3.1 Variable resistor specifics.

3.2 LabVIEW and Matlab Automation



Figure 3.6 Polarization Settings SubVI logo

An automatic procedure has been developed to collect the necessary data to compute the polarization curve. The procedure is set inside the “P F T Loop” and it’s composed of several cases inside a case structure. In this way if the user wants to acquire data for the polarization, the program will keep control on the other inputs. In the *Polarization Curve* section of the LabVIEW front panel interface, the user finds four elements: The *Polarization Logging Folder* path line, the *Start Polarization* and *Stop Polarization* buttons and a square LED named *Processing*.

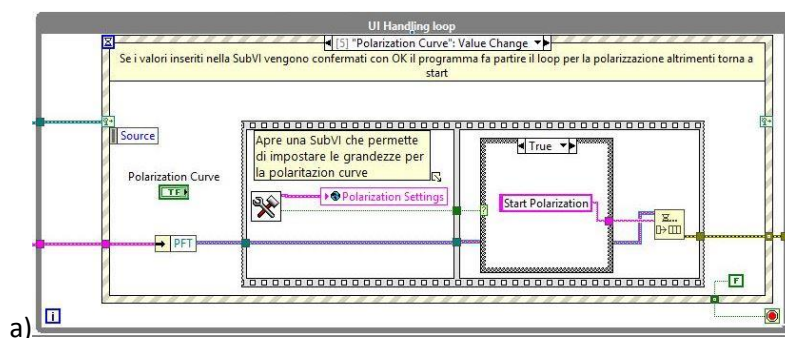
The folder indicator simply shows the path where the files are saved.

The Start button is programmed to start the polarization process shown in Figure 3.8.

The Stop button is programmed to stop the entire procedure at any point of the process. Whatever was done until this period remains saved.

The LED lights up when the process is running.

Figure 3.8. shows the flowchart of the procedure to collect data from LabVIEW. After the *Start Polarization* button is pressed the program calls a SubVI named Polarization Settings (refer to Figure 3.7) that opens a support window where the user can set several parameters: choose between Charge or Discharge and insert Flow Rate, Stack Voltage, Current Step, SOC and Max Current values. The *Cancel* button will make the program return to the default *Acquisition* case. The *OK* button will confirm the introduced values and make the procedure go on. Every step will make a different message appear in the “status” to inform what the program’s doing.



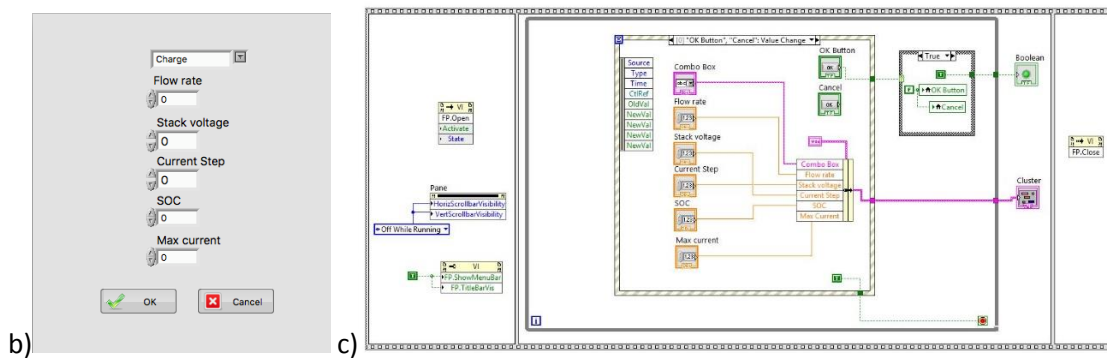


Figure 3.7 a) the Polarization case in the UI Handling loop, b) the window that allows the user to set the parameter for the polarization routine, c) the SubVI internal structure.

In the following, the listed cases of the flowchart are explained in detail.

- *Start Polarization*: it starts with the control of the active buttons (enable or disable), the setting of the current control to zero, and the writing of the set stack voltage on the voltage control. Every time the current or the voltage control are modified the user can check the actual value in the Power supply section on the front panel.
- *Wait 10s*: the procedure remains in control for 10 seconds. This allows the voltage in the cells to stabilize.
- *Add Current Step*: in a preliminary step, the actual current value, virtually added to the one of the current step, is compared to the max current value. The result enters a case structure. If it's true (lower) the loop can continue, otherwise it moves outside the loop because the set max value for the current is reached.
 - *"False" – Limit Reached*: there's control of the active buttons (enable or disable), setting of the current control to zero and the program gets back to the *Acquisition* case. A message will inform that the max current value is reached and the acquisition of polarization curves data ended.
 - *"True"*: Gives to the current control its new value.
- *Impose I*: the new value of current is imposed to the power supply.
- *Check*: if a voltage limit is set, the power supply is programmed to limit the output current. In this step it is checked if the output current reaches the set value or if it's limited by the power supply. The result enters a case structure.
 - *"False" – Impossible to Add*: there's control of the active buttons (enable or disable), setting of the current control to zero and the program gets back to the *Acquisition* case. A message will inform that the current can't be raised anymore and the acquisition ends.
 - *"True"*: continues with the loop.

- *Wait 5s*: the procedure remains in control for 5 seconds. It gives the command to the logging loop to start a parallel procedure in which a logging file is created and written.
 - *Title Polarization*: it creates the title of the file using the input values that the user set at the beginning of the procedure.
 - *Log Polarization*: Stack voltage and Current are written in the new .xls file.
 - *Stop Polarization*: the procedure ends.
- *Polarization*: in this case the program waits 10 seconds before giving the stop to the logging loop and make the procedure turn back to the *Add Current Step* case.

Once the procedure ends the program has created a set of files ordered in a folder. Their names indicate the date, the flow, the current and the SOC (e.g. '20171023 30 litri-min 8A SOC 40.xls'). For each current step, stack voltage and current are acquired several times during 10 seconds to make the measure as precise as possible so that a Matlab code was written to compute the average of these data and write all them in a new single file.

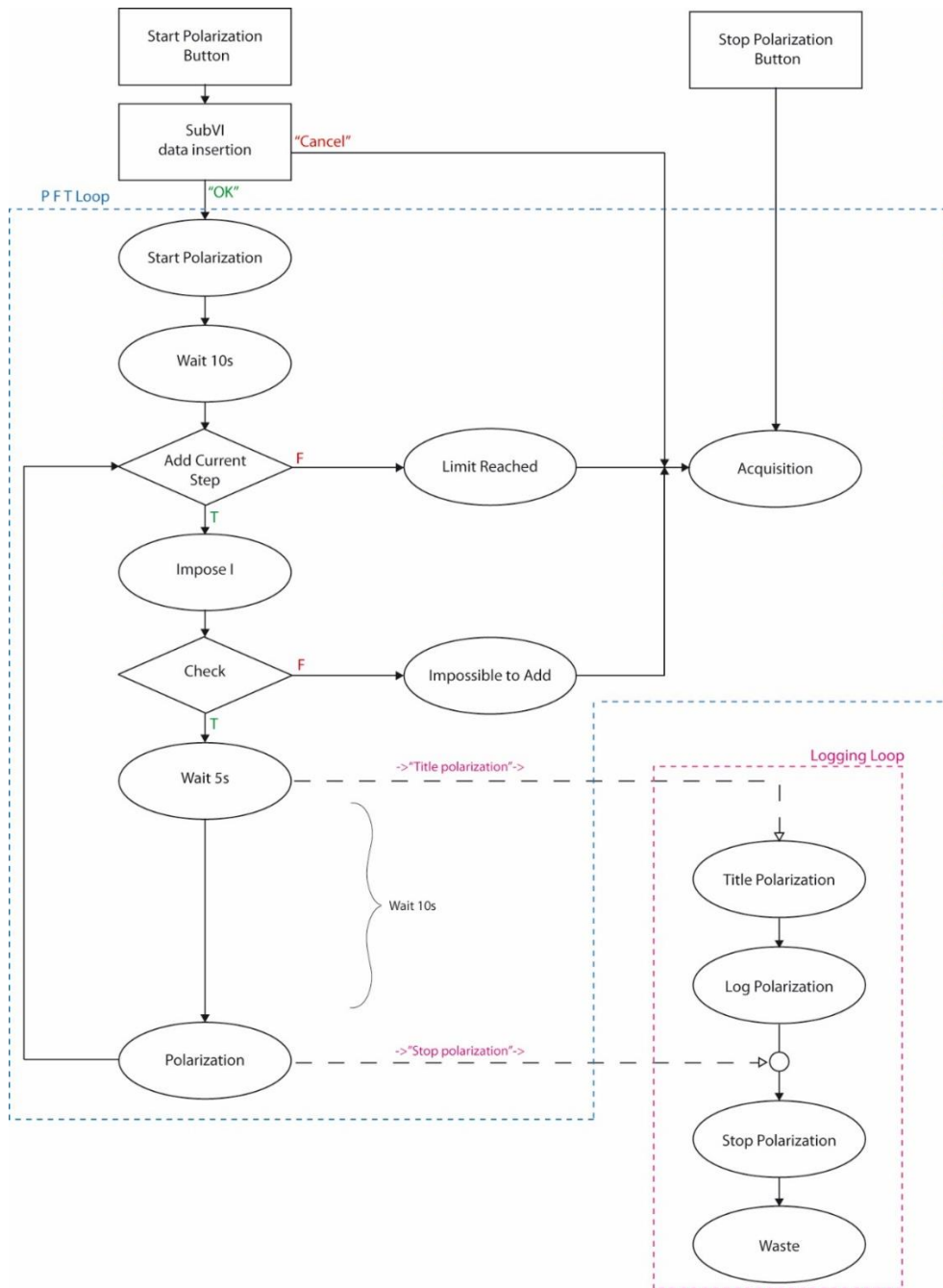


Figure 3.8 Flowchart of the automatic procedure to collect data for Polarization Curve computation.

Figure 3.9. Reports the general Matlab code to implement an automatic reading of the collected files to arrange them in a unique file for each SOC. The green comments help the user to understand what the program is doing and how to modify it according to every specific collection of data. Shortly, this code opens every data acquisition file, compute the mean value of the stack current and voltage and saves them inside a new file. The name of this file indicates SOC, charge or discharge and OCV. With the collected data it's than possible to represent the obtained Polarization curves for each state of charge of the battery.

```

1 % The program reads automatically the .xlsx files of the acquired values
2 % from LabVIEW, computes the mean values of stack voltage and current and
3 % writes them in a .xlsx file.
4 % Each measure is done by varying the current over a 2A height stepped path
5 % starting from 2A to a maximum of 70A.
6 corrente = 2;
7 i=2;
8 % Building the title of the measure files.
9 % Date(yyymmdd), flow (ff litri-min) and SOC(zz) values must be checked.
10 titolo1=('yyymmdd ff litri-min');
11 titolo2= ('A SOCzz.xlsx');
12 % Building the data file and its headers.
13 % The title specifies SOC (zz), if charging or discharging and OCV (b).
14 xlswrite('SOC zz carica/scarica OCV b', {'current (A)'} ,1,'A1');
15 xlswrite('SOC zz carica/scarica OCV b', {'stack voltage (V)'} ,1,'B1');
16 xlswrite('SOC zz carica/scarica OCV b', {'current LEM (A)'} ,1,'C1');
17 % The while cycle automatically stops when the "corrente" index reaches 71.
18 % It can be arbitrary set depending on the specific test limit for current.
19 while corrente < 71
20     strcurr= num2str (corrente);
21     titolo = sprintf ('%s %s', titolo1 , strcurr, titolo2);
22     % The program performs two different readings on the data files because
23     % LabVIEW randomly decides which set of data register first between the
24     % single cell voltages and the other measures so the desired data can
25     % be found in two different predetermined columns.
26     % It computes the mean and chooses the higher value between the two
27     % because the absolute value of stack current and voltage will always
28     % be higher than the single cell voltage one.
29     ReadV1 = xlsread ( titolo , 'Untitled' , 'BA2:BA22');
30     ReadV2 = xlsread ( titolo , 'Untitled' , 'L2:L22');
31     ReadC1 = xlsread ( titolo , 'Untitled' , 'BB2:BB22');
32     ReadC2 = xlsread ( titolo , 'Untitled' , 'M2:M22');
33     mediaV1 = mean(ReadV1);
34     mediaV2 = mean (ReadV2);
35     mediaC1 = abs (mean(ReadC1));
36     mediaC2 = abs (mean(ReadC2));
37     if mediaV1 > mediaV2
38         mediaV= mediaV1;
39     else
40         mediaV = mediaV2;
41     end
42     if mediaC1 > mediaC2
43         mediaC= mediaC1;
44     else
45         mediaC = mediaC2;
46     end
47     iesima= num2str(i);
48     cellacurr = strcat('A',iesima);
49     cellavolt = strcat('B',iesima);
50     cellalem = strcat ('C',iesima);
51     % Writing on the final file the set value of current, the mean stack
52     % voltage and the mean registered stack current.
53     % Always check that the final file name matches the one set before.
54     xlswrite('SOC zz carica/scarica OCV b', corrente, 1,cellacurr);
55     xlswrite('SOC zz carica/scarica OCV b', mediaV, 1, cellavolt);
56     xlswrite('SOC zz carica/scarica OCV b', mediaC, 1, cellalem)
57     corrente = corrente+2 ;
58     i=i+1;
59 end

```

Figure 3.9 Matlab general code which automatically analyses the data collected from LabVIEW.

3.3 Results

As mentioned in the first chapter of this section, different campaigns of data collections were done.

In the first campaign the polarization curves were plotted both in the case of charge and discharge at a high flow rate. Figure 3.10 shows the polarization curves obtained for eight SOC's in the charge mode of the battery for a current range spacing between 0 to 72 A (i.e. 0,12 A/cm²). As it can be seen the curves are almost linear and don't seem to follow the typical *s-shaped* profile. This can be due to sensible changes in the SOC during the charge process meaning that the concentration of the species in the electrolytes slightly changes during the collection of data. Moreover, it can be due to the fact that the studied range of currents fits only in the Ohmic loss region. Anyway, the good linear behavior is totally compatible with what should be expected from the central region of a polarization curve and it confirms that the collected data can be considered satisfying.

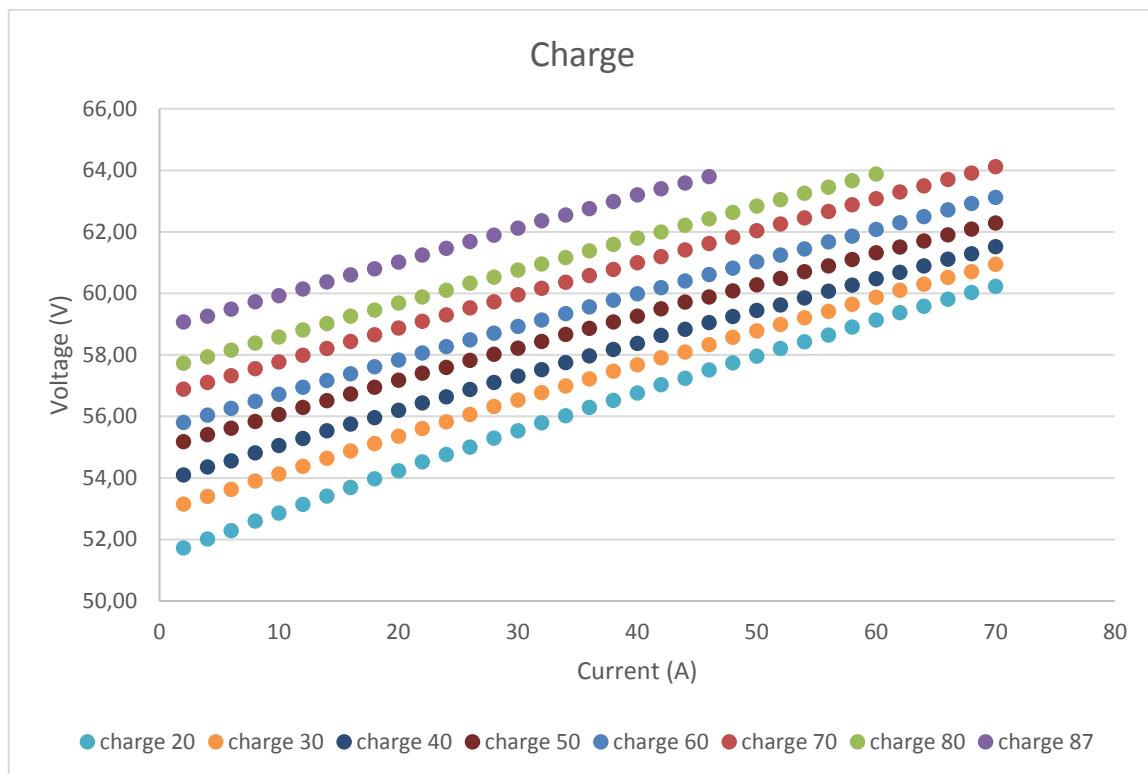


Figure 3.10 Polarization curves, charge, first campaign.

Of major importance are the data presented in Figure 3.11. In the left part of graph, the eight curves are the dual of the ones represented in the graph above and show the behavior of the stack while discharging with increasing current from 0 to 72 A. Since the stack constructor declared 72 A to be the maximum current the battery can purchase, the curves were expected to

fall drastically once this value was approaching. On the contrary, almost all of them maintain the linear behavior quite perfectly. So, to check the battery limits the passive load has been connected instead of the power supply and more points have been added. For 60% SOC, nine more tests have been performed with currents between 78 to 158 A (0,13 to 0,263 A/cm²). As it can be seen the curve's behavior is linear almost until 140 A and after this it slightly start to fall. The test could not proceed long after 150 A because it was the limit the contactor installed to disconnect the stack from the load was designed for. Anyway, these results show that 72 A were a precautionary limit while the stack performances and limits can be moved forward in current and power.

From an estimated power of almost 3,6 kW it can be projected to reach around 7 to 8 kW, while nominal currents can easily move around 100 A.

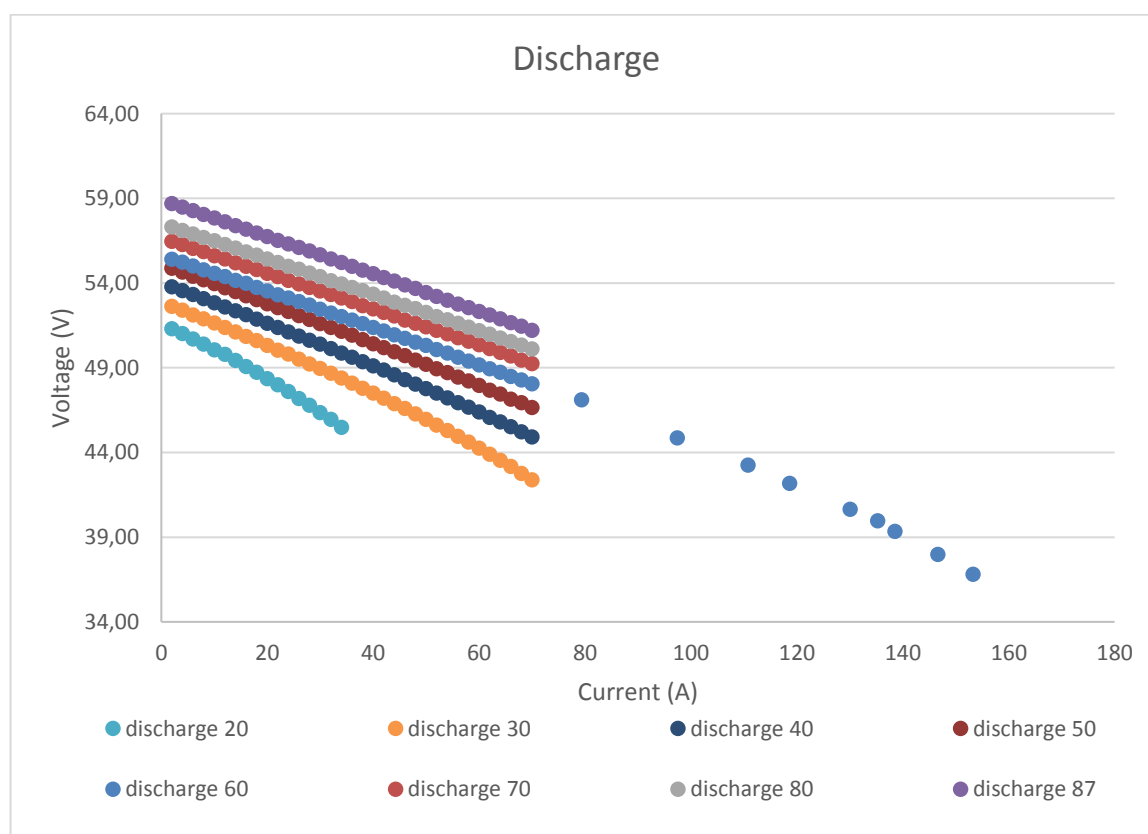


Figure 3.11 Polarization curves, discharge, first campaign.

In order to confirm the first-campaign data, some modification to the safety circuits have been applied and a new passive load was designed as described, to start a new data collection campaign. The results yet collected are here reported and commented.

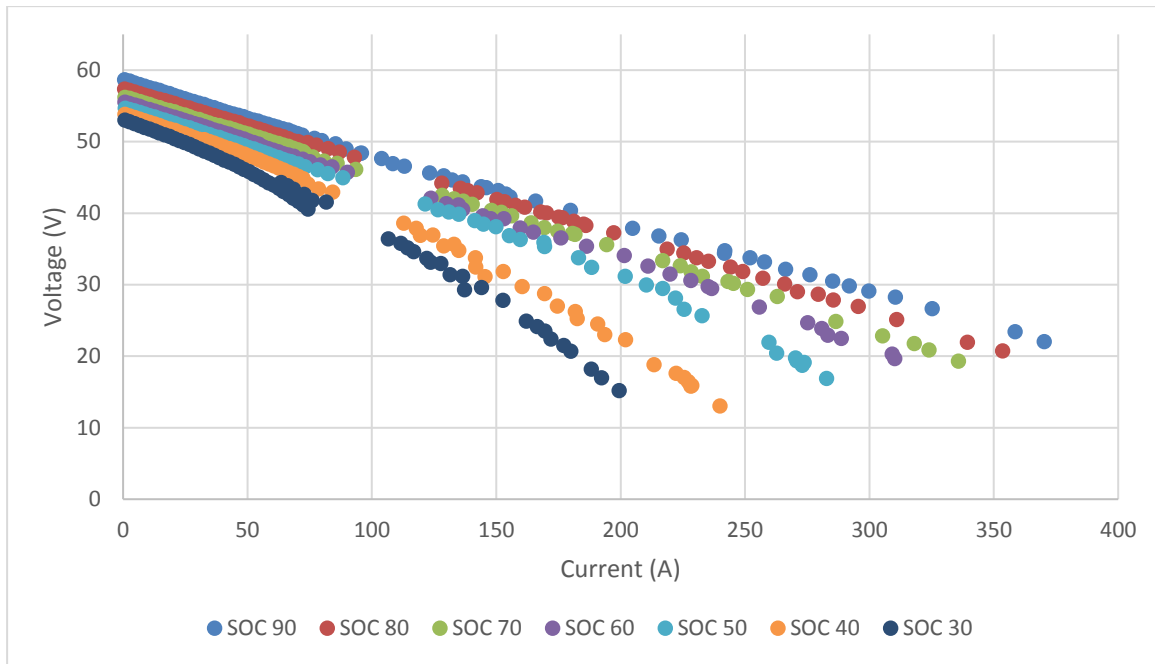


Figure 3.12 Polarization curves for different SOC.

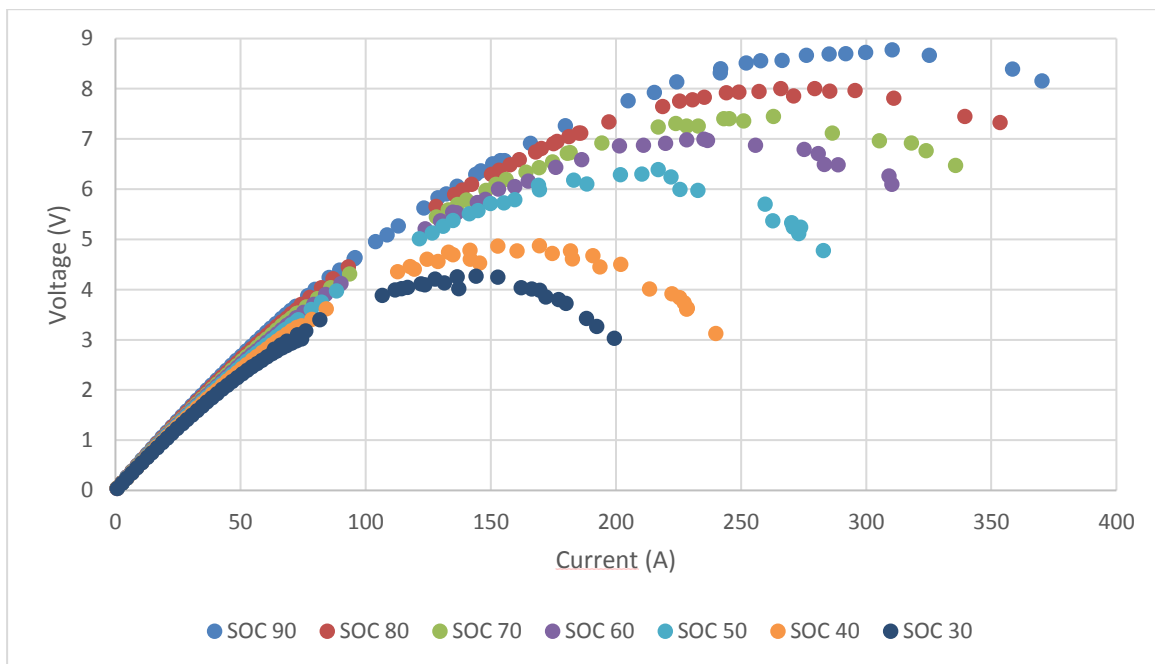


Figure 3.13 Power profiles for different SOC.

Figure 3.12 and Figure 3.13 show the complete polarization curves acquired in the second campaign of data acquisition and the corresponding power profiles respectively. As expected both the maximum declared current and power have widely been exceeded. In particular the current reached almost 380 A while the power has it maximum close to 9 kW at a SOC of 90 %.

The results are still under analysis and more data are needed to complete the set. As a preliminary comment, the fact that the curves in Figure 3.12 present a linear behavior is due to the thickness of the carbon felt electrodes. Since the active area is large, the activation energy tends to zero so that, for low currents, activation overpotentials are absent. On the other hand, for high currents, the effects of transport losses are not visible because the manual adjustment of the passive load wasn't instantaneous. In fact, even if the operation required a short time, during this period, the stack passed through a phase of open-circuit recirculation during which the previously reacted electrolyte has been replaced with fresh one. This fact in addition to the overfeeding of the stack, allowed the behavior to be majorly ohmic and so the curve to be linear.

Regarding the power, as expected from the first campaign, the declared limit of 3,6 kW has been widely exceeded for low SOC's as well.

4 Efficiency

In the case of a VRFB plant for research purpose it's of mayor importance to compute its efficiency in order to check how its behavior changes through time and which are the main factors that impact on its performances. First of all, three kinds of efficiencies can be computed: Round-trip efficiency, Coulombic efficiency and Voltage efficiency.

The Round-trip efficiency is calculated as the ratio between the energy given by the stack during the discharge and the total energy absorbed during the charge . Its value includes pump energy and all the internal losses in the battery. For a valid result, the charge and discharge processes must be done at the same constant current rate.

The Coulombic efficiency represents the quantity of charge given to the battery over the charge the system can yield during its discharge. It can be easily computed by integrating the input and output current in time.

The Voltage efficiency is computed as the ratio of the average discharge voltage to the average charging voltage [23].

4.1 LabVIEW Automation

The LabVIEW Automation routine was developed giving the possibility to the final user to compute the energy absorbed or given by the plant while continuing to acquire and control all the other signals. The procedure can be controlled both manually or automatically. The program is in fact designed to stop automatically when a certain SOC is reached or it can be interrupted at any time by the user by simply clicking at a button.

The routine controls can be found in the *Efficiency* window in the front panel. It is composed by several elements: The *Start Efficiency* and *Stop Efficiency* buttons which make the procedure start or stop respectively, *SOC Charge* and *SOC Discharge* numeric indicators, a time indicator called *Efficiency Running Time* and a status window.

The two numeric indicators show the limits set by the user that must be reached by the battery after the charge or discharge process.

The two buttons make the routine to start or to stop by sending a command to the "Handling Loop" section. When the start command is given LabVIEW launches a dedicated SubVI and an additional window opens. Here the user can set several parameters: firstly, the user is called to choose between *Charge* or *Discharge* depending on the modality imposed by the power supply.

Then, based on the previous selection the Charge or Discharge cell enable and so the user can introduce the SOC it wants the battery to reach. Finally Stack Voltage and Current must be introduced. The Power Supply is designed to work as follow: once voltage and current are set and imposed, it gives the battery a constant current but if the voltage limit is reached it automatically gives the battery less and less current. So, the charge or the discharge processes are performed at constant current and then at constant voltage. The *OK* button will confirm the introduced values and put them inside a Global Variable (GV), the *Cancel* one will make the program go back to the default Acquisition case.

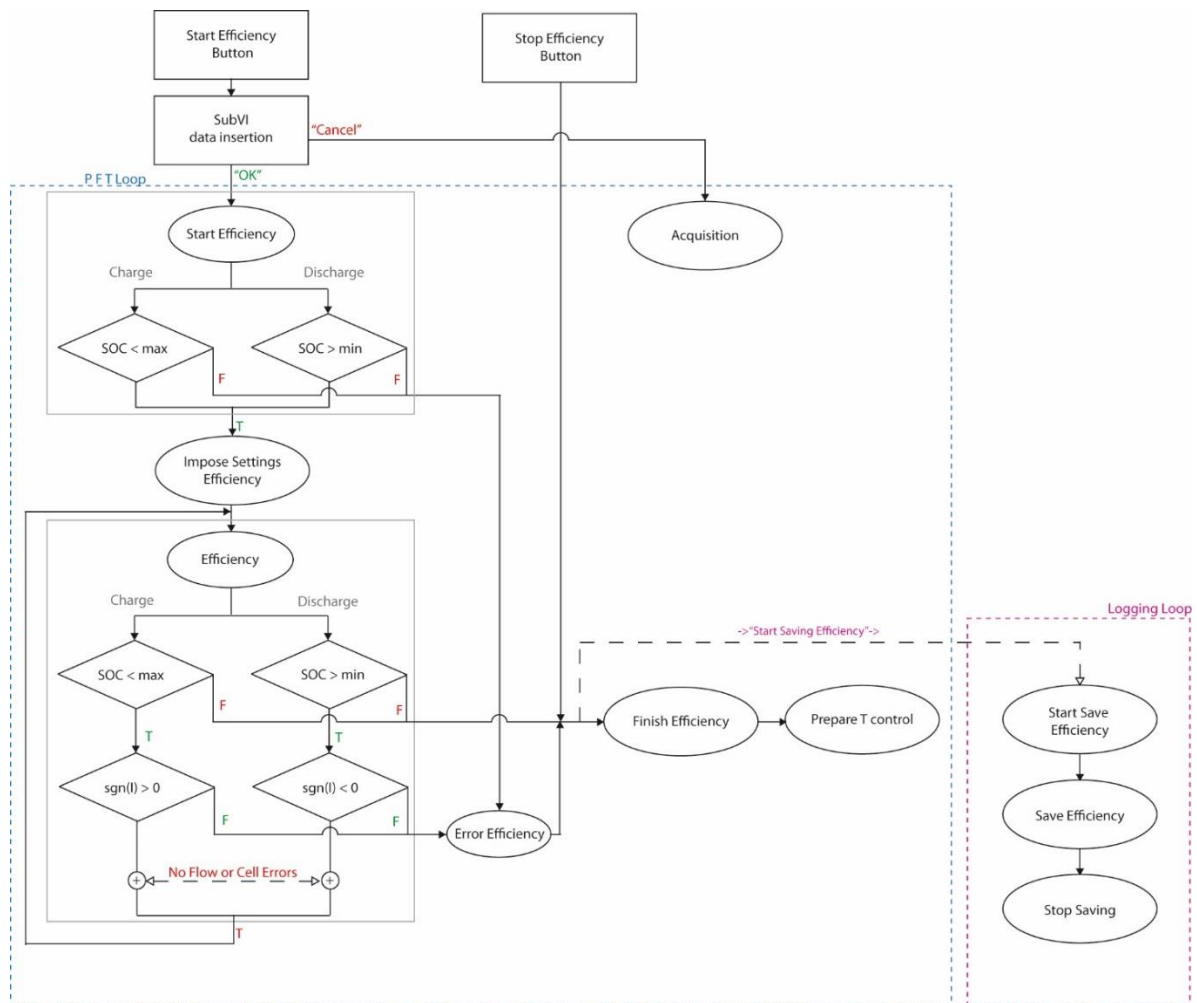


Figure 4.1 Efficiency routine flowchart.

Figure 4.1 shows the flowchart of the routine. The whole process is complicated by the presence of several security layers. As a matter of facts, the high energy the device can store makes the charge and discharge process very long and delicate so there must be a way to keep it under

control. Problems connected to the over-charging or over-discharging of the device can be the corruption of the electrodes or the formation of hydrogen that must be totally avoided.

The following list explains in detail the step of the Efficiency routine.

- *Start Efficiency*: time is recorded and memorized in a shift register. Some buttons and windows are enabled or disabled. Stack Voltage and Current are taken out of the GV and written on the respective controls. A preliminary check on the introduced data is made by confirming that SOC's are coherent with the actual status of the battery (e.g. OK if the battery is at 20% and the command is to charge it up to a higher value like 90%, Error if the battery is at 20% and the command is to charge it up to a lower value like 10%. The dual case in the case of discharge). If any error is detected the routine shifts to *Error Efficiency* otherwise the Efficiency acquisition process can go on.
- *Impose Settings Efficiency*: if no errors were detected, in this case the procedure imposes the set values of current and voltage to the power supply.
- *Efficiency*: this case is subdivided into two subcases one for the Charge and one for the Discharge. In the following, the Charge case is explained in detail and the Discharge dual values are written in brackets. Inside the case, some operations are done continuously while others follow a sequential structure. In particular the pump control made with PID, the computation of the integrals and of the running time are independent so that they are done every time the routine calls for this case to happen.
 - *SOC < MaxSOC?*: This first case checks if the set maximum (or minimum) limit of charge is still above (or under) the current state of charge. If this is true, it means that the battery needs to be charged (or discharged) more and so the procedure can follow. On the other hand, the program will go to the *Finish Efficiency* case meaning that the whole process of charge (or discharge) has come to an end and the collected data can be stored. (In the discharge case the question is *SOC > minSOC?*)
 - *Sign(I) > 0?*: This intermediate case it's necessary because if inadvertently the user chose for example the "Charge" setting but the power supply is in "Sink" or "Discharge" mode, even if the current SOC is lower than the maximum expected, the battery will never reach it. In fact, it will decrease instead of rising. According to the operational mode of the power supply (Source or Sink) the current is registered as positive or negative. In the case of Charge the current is expected to be positive so if its sign is positive no error is present. In this case, even if the answer to *sign(I) > 0* is "true" a "false" output is generated. This was made because the following step accept as an input to continue the procedure a "false" value, meaning that no error is present. Additionally to the current sing input, the next case structure receives as an input the flow meter and the cells

voltages values. For the flow meter the “false” output is generated when the flow is higher than a preset value, for the cells voltage it’s “false” if none of them overcome 1,7 V. If all of them are “false” the procedure will continue by simply coming back to the *Efficiency* case and repeating the double check procedure again, otherwise if just one of them is “true”, stack current and voltage are set to zero and the routine will follow to *Error Efficiency* case. (In the discharge case the question is $Sign(I) < 0?$).

When the Finish Efficiency string is enqueued inside the PFT loop queue, the Start Log Efficiency string is sent to the Logging Loop queue, giving it the command of starting the procedure to store the collected data in a .tdms file.

- *Error Efficiency*: when called, the case shows two error messages to the user. One in the status string indicator in the Control Panel section which will disappear after few seconds and inform the user saying “UNCORRECT SET VALUES – SOC is higher or lower than the current one or Power Supply’s working in incorrect mode”. The second one appears in a string indicator in the Efficiency section of the Front Panel warning the user that “Error Occurred, Check Settings or Power Supply mode”. This message won’t disappear until the Start Efficiency button is pressed again or the program is restarted in order to allow a longer check of the status of the Efficiency routine. Even if some error occurs the program automatically starts the procedure to save the data.
- *Finish Efficiency*: after enabling or disabling some buttons and indicators, the case stores the collected data inside the data saving queue: Time Efficiency by subtracting the current time to the one registered at the beginning of the procedure in the Start Efficiency case, Stack Energy, Pump Energy and Hydraulic stack catholyte and anolyte energy losses which are converted in Wh by dividing them by 7200, Current, Initial and Final SOC, Stack Coulomb charge and Voltage efficiency which is the mean value of the voltage during the charge or discharge process. As a matter of fact, every iteration of the while loop is done imposing a wait time of 500ms. If no wait time is given to the program, the iteration time is not constant so, for the fact that the LabVIEW integration tool works with samples and not with time steps, the obtained result is based on a samples scale and not on a time domain. Once done, the program switches to the Prepare T control case and the whole system is put in Stand-by mode controlling the temperature. Together with it, the Logging Loop cycle goes to the Start Save Efficiency case.
- *Start Save Efficiency*: in this case the .tdms saving file is created and opened in the file path where the VI is saved.
- *Save Efficiency*: Time Efficiency and all the energies data together with the set Current, the initial SOC and the final SOC are written in the file.

- *Stop Saving*: the data queue is emptied to avoid future overwriting and it closes the .tdms file.

Whenever, during the procedure, the user can stop the acquisition and save what's computed, simply by clicking the *Stop Efficiency* button. As shown in the flowchart (Figure 4.1) the loop will move to the *Finish Efficiency* case and then it will follow as previously described.

4.2 Results

The results here presented refers to a data acquisition campaign made with a software version where only the Round Trip Efficiency was computed. After this test, the software has been upgraded to the version presented in the previous chapter, but a data acquisition hasn't yet been done. The efficiency should be performed by charging the battery from a very low state of charge to a maximum set SOC or to one given by the cells' voltage safety limit of 1,7 V. When this value is reached, the constant current charge stops and the discharge process, at the same current rate, starts. The process ends when the battery reaches the initial low SOC. In the first test performed, due to one cell's uncommon behavior, the discharge process was stopped before the battery discharge completely. An assessment on how the process should end was done based on the trend of SOC as a function of time. In particular it was supposed the battery to finish the discharge with a constant output voltage and current of 44 V and 60 A respectively. Table 4.1 and

Table 4.2 report the data from the charge and discharge processes.

Time (h)	Current (A)	Initial SOC (%)	Final SOC (%)	Stack Energy (Wh)	Pump Energy (Wh)	Tot Energy (Wh)
6,6261	60	4,72	91,99	25009,63	1475,30	26484,93

Table 4.1 Efficiency data during charge.

Time (h)	Current (A)	Initial SOC (%)	Final SOC (%)	Stack Energy (Wh)	Pump Energy (Wh)	Tot Energy (Wh)
5,2064	60	92,83	20,10	14989,90	1122,65	13867,25
5,5	60	92,83	5	15789,90	1188,65	14601,25

Table 4.2 Efficiency data during discharge. In the second row there are the collected data, in the third row there are the projected data.

$$\text{Round Trip Efficiency} = \frac{\text{Stack Energy}_{\text{Discharge}} - \text{Pump Energy}_{\text{Discharge}}}{\text{Tot Energy}_{\text{Charge}}} \quad (17)$$

By using equation (17), the resulting Round trip efficiency is 52,36% in the case the final SOC would be 20,10% or 55,13% if the estimated values of energies are considered.

For what it concerns the charging process the results accomplishes the expected values of 24-26 kWh for the stack.

Figure 4.2 shows the trend of SOC as a function of time during the charge and the discharge processes. Still, it is not so clear why the shape of the curves is non-linear and more research is needed.

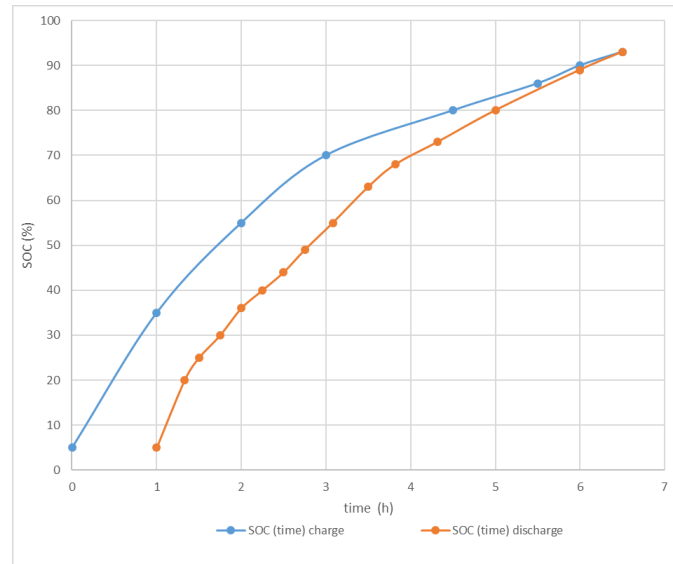


Figure 4.2 Behavior of SOC (time) for charging and discharging.

Further campaigns will acquire more data for different currents and flows configurations and more results will be presented over the efficiencies of the test facility.

5 Temperature Control

As written at the beginning of this essay, the temperature control is a critical part in the management system of a VRFB plant. Researchers nowadays ([24], [23], [4], [25]) are interested in the study of the electrolyte behavior in order to extend the temperature interval of stability together with the possibility of rising the vanadium concentration and so the whole battery's capacity.

Chemical properties of vanadium solutions are still not well understood including the compounds this metal creates in sulfuric acid solutions [24].

At the earlier stages of research, Skyllas-Kazacos and her group at the UNSW [26] found out that both positive and negative electrolyte solutions suffer from precipitation respectively at high and low temperatures. As a matter of fact V(II) precipitate at a temperature of 10°C or lower while V(V) start precipitating over 40 to 50°C. This fact is limiting the VRFB to a certain range of working temperatures. The precipitation process is a function of lots of parameter including temperature, time and concentration of species. The latter is a chemical limit which intrinsically limit the solution of any salt in a solvent. Each of the four vanadium oxidized states compounds has its own solubility limit which must be taken into account, together with its viscosity, density and specific heat considering the electrolytes to be a mixture of two species at the same time. Concentration and temperature are related because as the molarity of a solution rises, the precipitation temperature lowers. In order to achieve a greater temperature range, a lower ion concentration is required although this reduces the specific energy [6]. Gareth Kear and his team in [12] demonstrated that increasing the temperature lead to a better voltage efficiency due to the rise in the electrolyte conductivity and increased reaction kinetics.

In 2009 Rahman and Skyllas-Kazacos published a study over the possibility of using supersaturated V(V) solution for the positive electrolyte [25]. They observed that the solution presents a pretty stable temperature behavior using up to 5 M V(V) in 6 M sulfate solution. This was an important study demonstrating that it is possible to extend the concentration range and so the energy density, but more parameters must be considered such as the solubility of other vanadium states and more studies were suggested.

In 2011 the UNSW team [5] managed to optimize the solutions containing 2M V(V) in 4 to 5 M of sulfuric acid. In the same year, Liyu Li et al. [4] successfully widen the temperature range to -5°C to 50 °C by using a mixed sulfate-chloride electrolyte with a vanadium content of up to 2.5 M. The vanadium redox couples were seen to improve their reaction kinetics while remaining stable and keeping a high level of efficiency.

The behavior of the VRFB at high temperature is more important than the one at low temperature because in this electrochemical device, internal discharge and ohmic losses (due to shunt currents) as well as self-discharge reactions, are exothermic processes accompanied by a liberation of heat which will eventually heat up the whole system.

A very recent study [24] over the effect of temperature and composition on catholyte stability, managed to extract from experimental observations a model which express the induction time as a function of vanadium and sulfate concentrations and temperature. In the experiment they set some samples of electrolyte with different composition in a thermally stable solution and registered the time after the precipitation start occurring. They demonstrated that the behavior is connected to an activation energy which remains constant in a range of temperature between 30 to 60°C and for V(V) concentrations between 1.4-2.2 M and sulfate concentration between 3.6-5.4 M. The model's described by equation (18).

$$\tau = \tau_{std} e^{m\left(\frac{1}{T} - \frac{1}{T_0}\right) + \beta_s([S] - [S]_R) + \beta_{V5}([V^V] - [V^V]_R)} \quad (18)$$

Where

- τ is the induction time,
- $[S]$ is the concentration of sulfate solution,
- $[V^V]$ is the molarity of the vanadium V(V) in the solutions,
- T is the temperature expressed in K.

In our case the solution has a constant sulfate concentration of 4.5 mol⁻¹dm³ while the vanadium V(V) molarity depends on the SOC. When the battery is completely charged the SOC is 100% while V(V) is equal to 1.6 mol⁻¹dm³. In Table 5.1, all the other parameters are listed.

τ_{std}	7. 9226 * 10⁶ [s]	Standard induction time
m	2.0785 * 10⁴ [K]	Slope of Arrhenius plot
T_0	298.15 [K]	Standard temperature
β_s	2.073 [mol⁻¹dm³]	Sulfate concentration parameter
β_{V5}	-3.434 [mol⁻¹dm³]	V(V) concentration parameter
$[S]_R$	4.5 [mol⁻¹dm³]	Standard catholyte sulfate conc.
$[V^V]_R$	1.7 [mol⁻¹dm³]	Standard catholyte V(V) conc.

Table 5.1 Induction time equation (18) parameters.

Figure 5.1 reports the graphical representation of induction time as a function of SOC and Temperature as stated by equation (18).

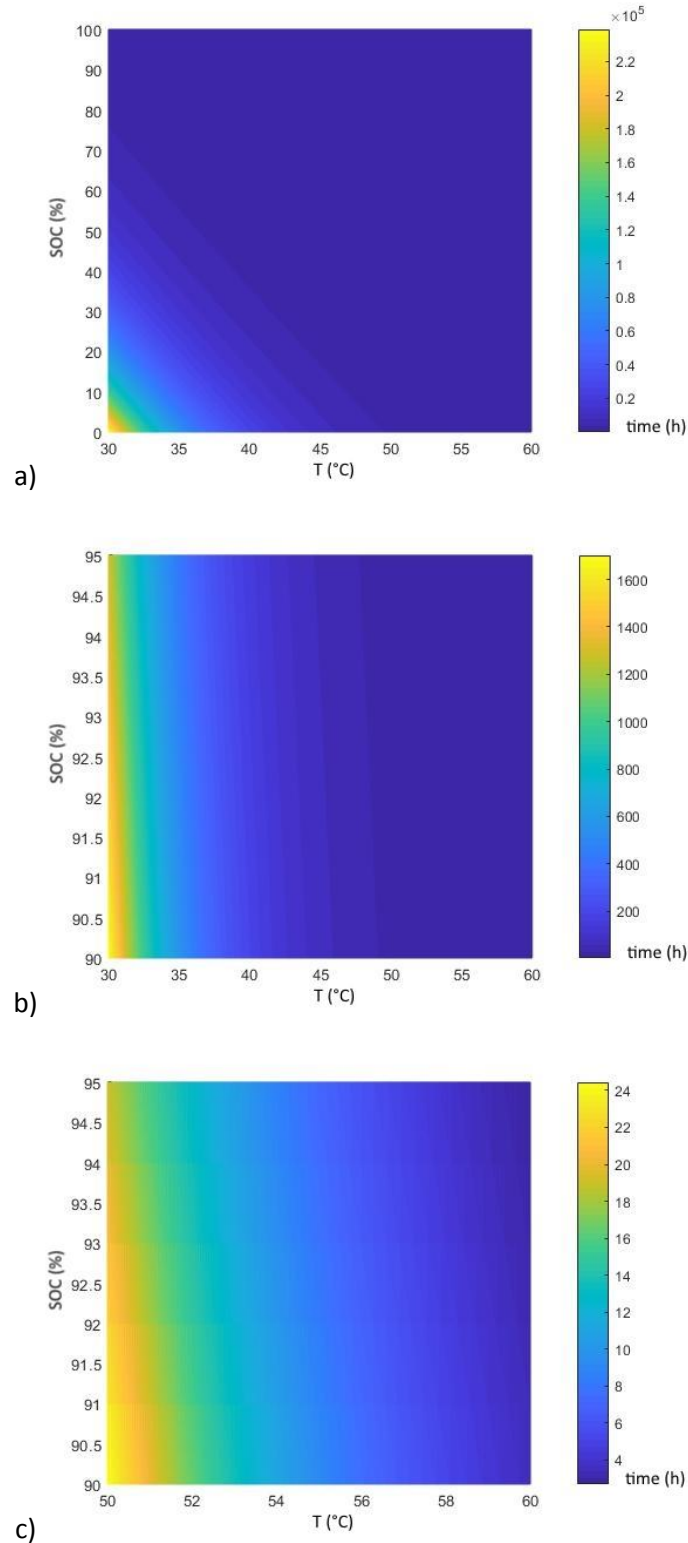


Figure 5.1 Graphs of induction time as a function of SOC and Temperature following equation (18). a) $T = 30$ to 60°C , $\text{SOC} = 0$ to 100% , b) $T = 30$ to 60°C , $\text{SOC} = 90$ to 95% , c) $T = 50$ to 60°C , $\text{SOC} = 90$ to 95% .

Figure 5.1 a) shows the induction time values for the V(V) electrolyte solution present in the ESLab in the range of validity of equation (18). It can be noticed that no interesting data are coming from this analysis being the solution for both low temperatures and SOC stable. So, in b), the analysis was concentrated between 90 to 95% of SOC but keeping the range of temperature from 30 to 60°C. Still the induction time scale let us assume that for low temperatures, even if for high SOC, the solution can be considered stable. Finally, in c), the investigation shifted to high values of temperature (from 50 to 60°C). In this case it can be pointed that the maximum induction time depicted is 24 hours, so that, this graph sets the limits for a one-day long stand-by. The analysis coming from this study reveals that in stationary conditions, that is if the solution is let without any kind of external heat source, it can be considered stable since high values of temperature or SOC.

This opens to the possibility of modifying the actual stand-by algorithm passing to an adaptive one in which current SOC and temperature are monitored to program a recirculation of electrolyte when it is strictly necessary. In this way the solutions, which slightly self-discharge when recirculate inside the stack, can maintain their charged state for a longer time and so the battery efficiency can reach higher values.

More accurate studies about the kinetics of the self-discharge reactions are needed as well as the behavior of the electrolytes when heated by an external heat source to produce an accurate model.

6 Aging Effects and MRO

6.1 Dismantling and check operations

After one year of operation, the stack was submitted to a maintenance, repair and operations (MRO) procedure to check if any detriment of material or problem arise from the inspection. The whole operation was planned in detail in advance.

Firstly, the lab was prepared to allow every operation to take place safely. The red hydraulic press was equipped with a specially designed aluminum rack which can host the stack during the dismantling operations (Figure 6.3).

During the first phase, all the appendix devices where alit from the stack, namely the LEM current transducer and the safety fuse. The cables connecting each cell to the corresponding measure line were disconnected and marked for future reconnection. All the bipolar plates holders were marked with the same number of the cable. The horizontal extrusion holding lights and some cabling was moved and all was stored separately (Figure 6.1).

In the second phase the Mix valve on the front panel of the stack was removed, emptied from the remaining electrolyte in its inside and stored separately. No leakage has been detected between the valve and the PVC front panel (Figure 6.2).

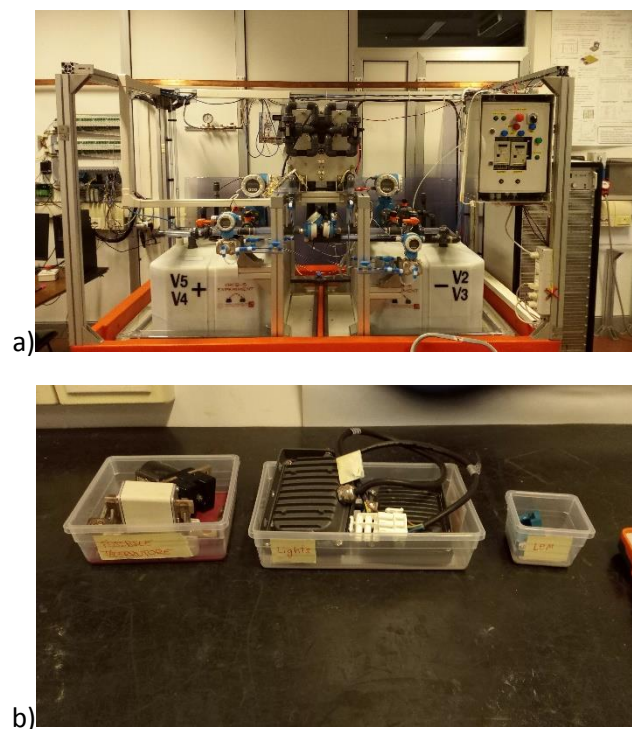


Figure 6.1 a) Plant after the first phase: OCV cell, LEM and horizontal upper profile removed, b) the removed objects accurately separated.

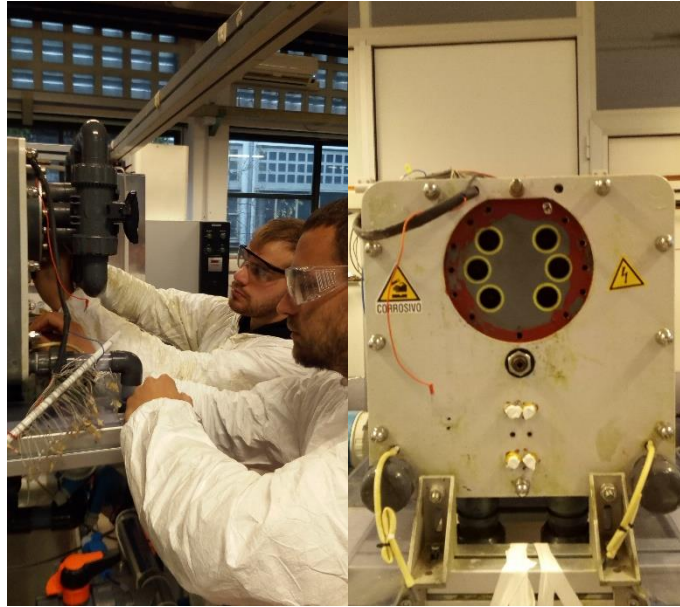


Figure 6.2 Second phase: the mixing valve is dismantled from the frontal panel.



Figure 6.3 Aluminum rack and hydraulic pressure jack.

When the stack was free from any cabling, connection and devices, (phase three) the yellow lifting crane of Figure 6.4 a) was used to move the stack from its plant position and transfer it to the aluminum rack horizontally to be then turned vertically with its front face down (phase four). Once the moving operations ended, some electrolyte leakages have been detected close to the solutions inlets. As it can be noticed from Figure 6.5 a), blue crystals formed consequently to the leakage of V(IV) solution from bad sealed plates. These residuals have been adequately cleaned and a first visual inspection on the external health-state of the plates was performed detecting any harm. After this, wooden clips have been applied as shown in Figure 6.5 b) and c) to keep the plates sticking together once the stack would have been disassembled.

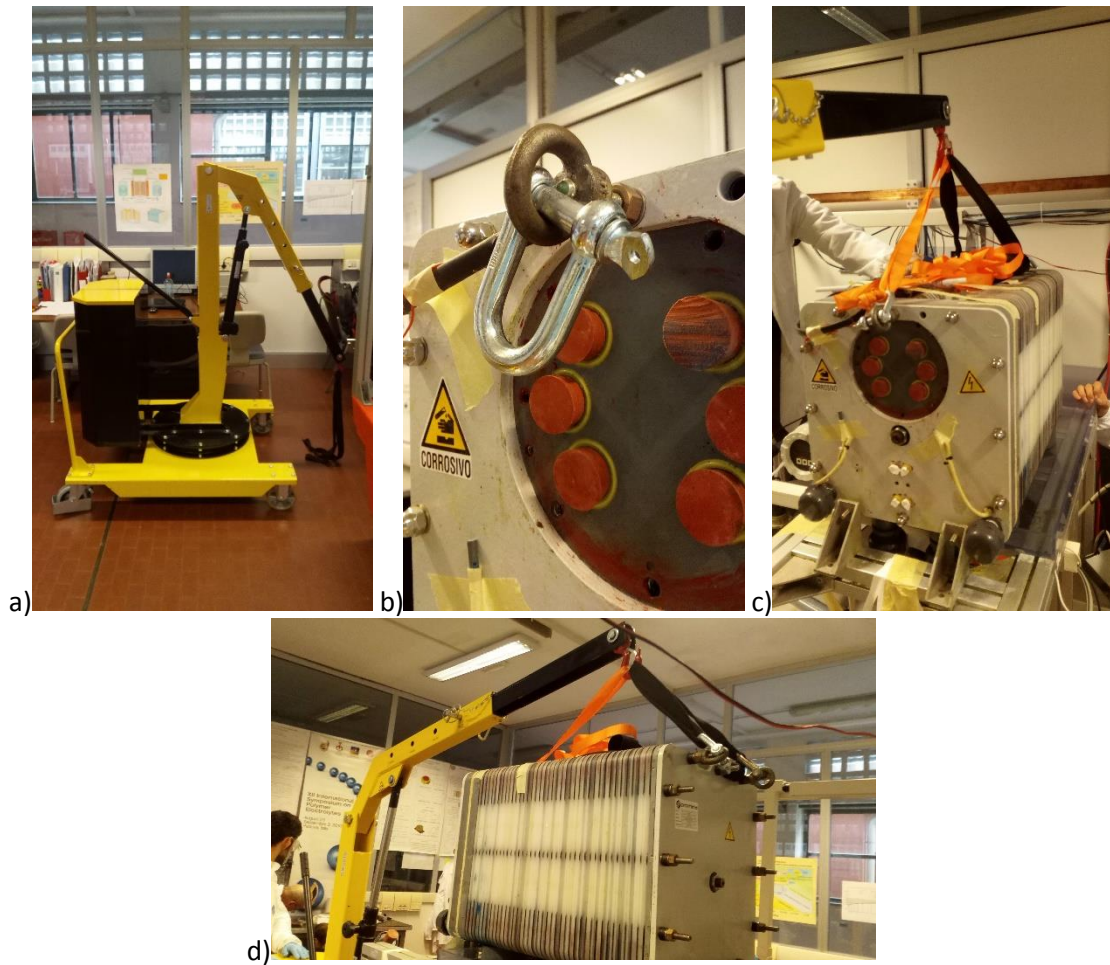


Figure 6.4 Third phase: the stack's hung and moved with a crane and placed horizontally.

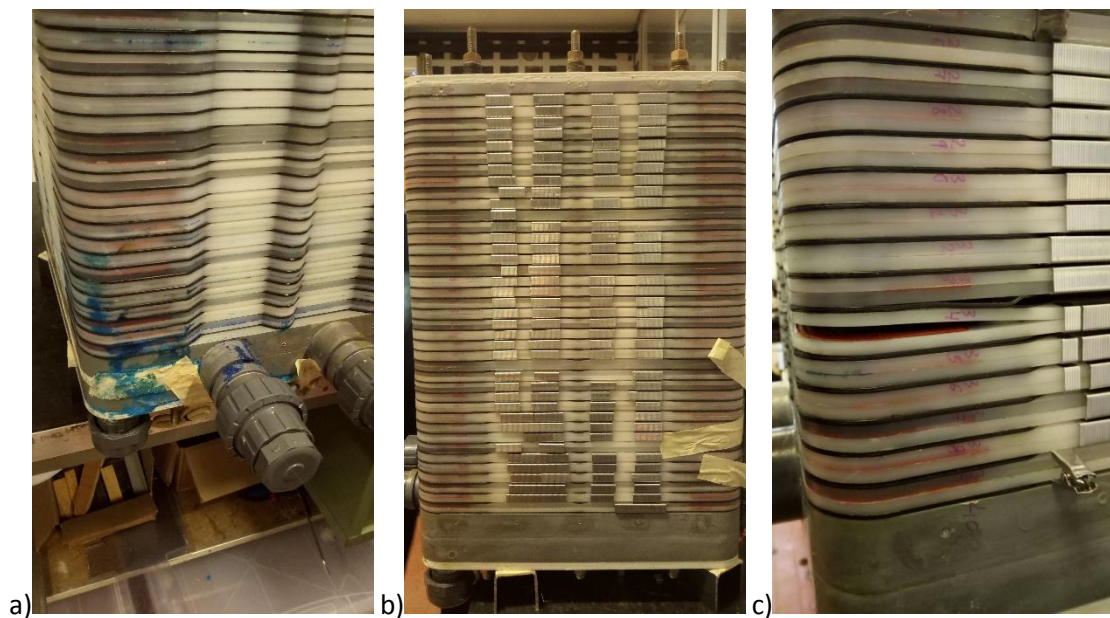


Figure 6.5 Fourth phase: the stack's turned vertically. a) some electrolyte leakage is detected from the bottom part, b) wooden clips are applied to avoid polypropylene plates to open completely as it can be noticed in c).

During the fifth phase the MEAs assembling the stack were separated and each component has been stowed in distinct boxes after been visually checked. The first detected issue was the presence of small PVC shaving blocking some of the manifold inlet channels. Their presence is justified by the fact that previous maintenance operations on the PVC head of the stack were performed and not all the drilling residuals have been removed. This was not representing a big deal for the VRFB performances because the shavings were covering just partially the plates' inlets. At a first sight, none of the components underwent deep wear or irreparable damages due to operation conditions (Figure 6.6).

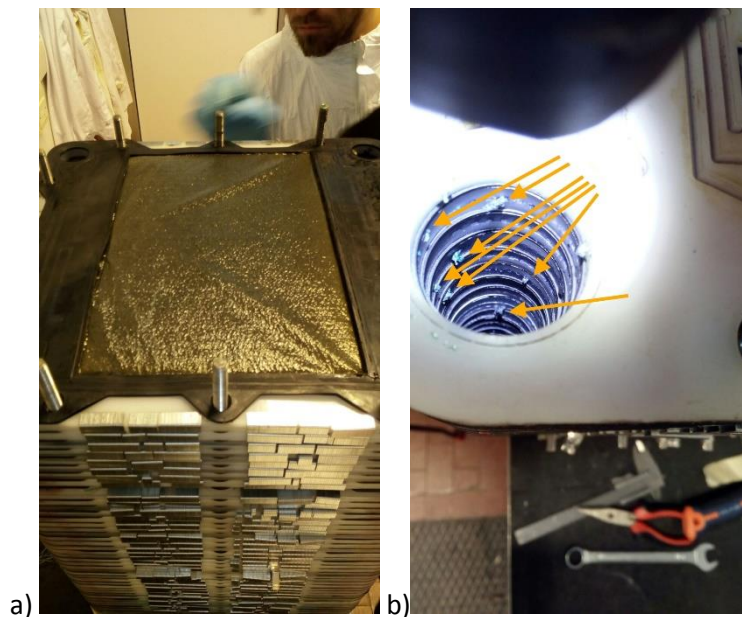


Figure 6.6 Fifth phase: MEA disassembled and preliminary visual check. In b) some manifold channels are blocked up by PVC shavings due to previous drilling maintenance operations on the head plate.

In the sixth phase the metal plate has been removed from the frontal PVC plate and a gas sealing test has been performed after some leakage were detected. The test showed any consistent sealing loss meaning the vanadium solution came from secondary unprecise bonding made during the panel construction. The acid solution didn't produce any harm to the metal plate when in contact with it.

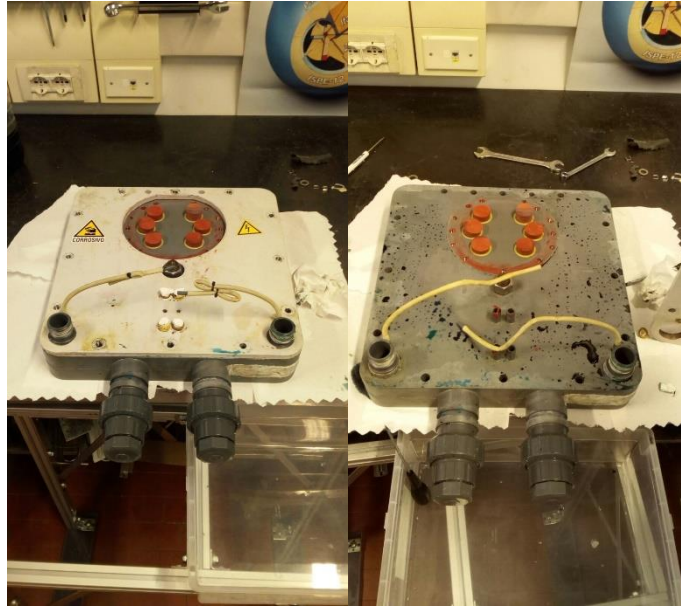


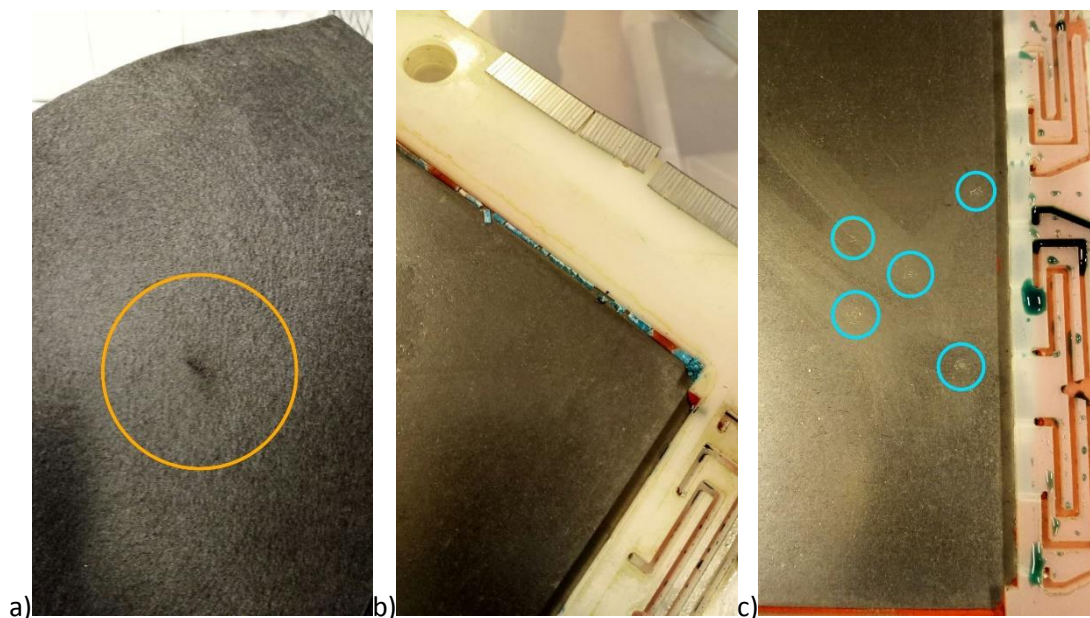
Figure 6.7 PVC frontal plate is divided from its metal where more electrolyte leakage are detected.

The seventh phase was devoted to a more accurate check on the components conditions. The bipolar plates have been washed with bi-distilled water from any eventual electrolytes residuals and the sealing of the acetic silicon and the state of the graphite plates have been checked. The flaws detected are described and commented below.



Figure 6.8 Seventh phase: each MEA is divided and each bipolar plate is washed with bi-distilled water and accurately examined.

Figure 6.9 reports all the flaws noticed on the MEA components. Firstly, in a) it can be seen a hole in one of the carbon felts. Few of them reported this kind of injure which was, most probably, already present during the assembly of the stack. In b), it is shown the behavior of the acetic silicone when immersed in a corrosive environment and subjected to an electric field. The elastic red paste is transformed into a mealy white compound wetted with blue electrolyte. Its consistency is impalpable and it disrupts easily by simply touching it but anyway it seems nor to compromise the sealings nor to create problems by blocking the electrolytes inlets. c) shows some point defects on one of the bi-polar plate while d) shows a linear bending scratch. Several plates presented one or both of the injures (in the form of single or multiple point or as a linear scratch). These flaws haven't been related to any incorrect treatment of the battery but simply to local imperfections of the material already present in the mounting process. This is corroborated by the fact that previous direct observations of corroded plates, were showing a different kind of damage on them and any malfunction was observed in any of the cells affected by the flaws of c) or d). Lastly, e) and f) show the deposition of carbon material on the bottom side of a bi-polar plate. This phenomenon has been observed in few plates and it resulted in a little detriment of the carbon plate covered with the deposit. The precipitated wasn't occluding any hole of the inlet manifold and seemed not to affect the performances anyhow. Once removed, any other effect on the plate has been observed.



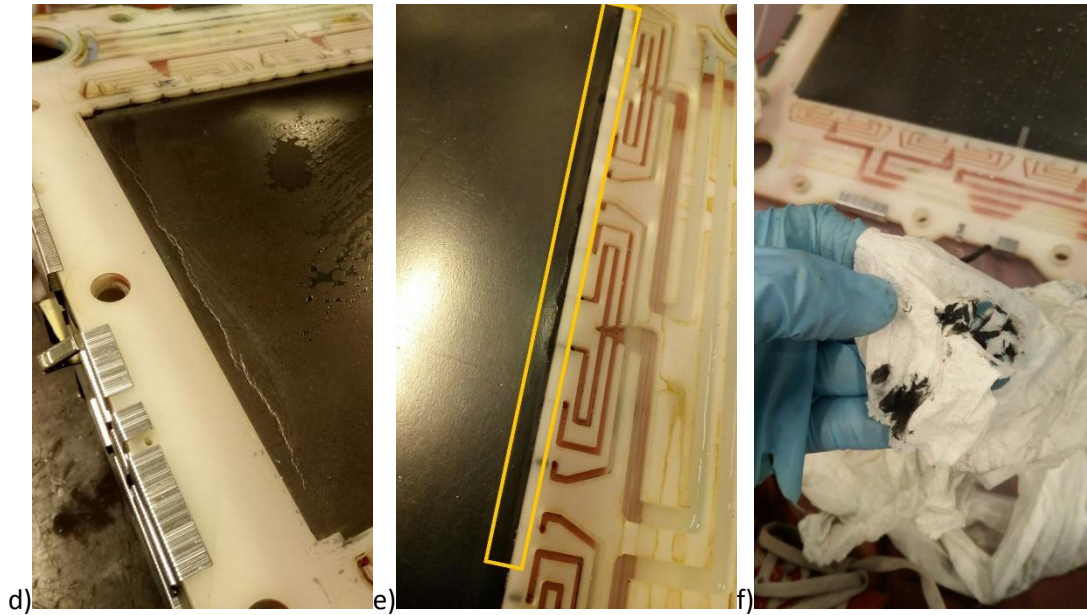


Figure 6.9 Some of the flaws found on the plates. a) a carbon felts' hole, b) acetic silicone behavior in presence of corrosive environment and electric field, c) and d) imperfections on bipolar plates surface, e) and f) carbon felts' deposit close to the plate's inlet.

A further aging effect has been observed in 10 plates and it was pointed as the cause of leakage shown in Figure 6.5 a). This was the untighten seal of the acetic silicon due to several possible factors. Firstly, because acetic silicone was not the most adequate choice to bond together the two plates. Secondly, even if the silicone was deposited by an industrial plotter, the lines in the polypropylene structure were not suitably and cleverly carved to ensure a perfect deposition of silicone, a consequent bonding between plates and sealing to prevent leakage. In fact, as shown by Figure 6.5 c), plate 34 was opening around the main electrolyte inlet but thanks to the clips the two halves didn't separate completely. Although a perfect bonding was not necessary because the whole stack components are subject to a consistent pressure during normal operation, however a flawless sealing created by the silicone is necessary because the electrolyte flowing in the stack is pressurized compared to the external atmospheric pressure.

Carbon felts were not subject to a deeper analysis than the visual one, but their status was reported to be satisfying.

Regarding the membranes, all of them present no visual injures or irreversible damage due to working conditions nor consistent aging effects.

6.2 Reassembly operations

The procedure to reassemble the stack and to settle it back to the original position is here described.

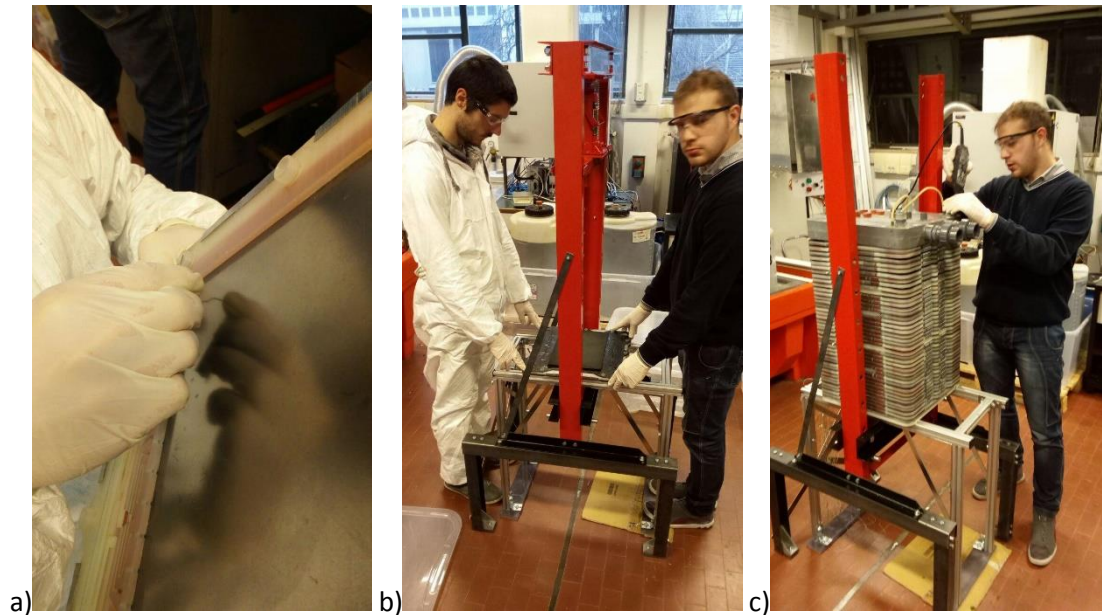


Figure 6.10 Reassembly procedure's operations. a) a final and accurate check on the manifold's holes status. b) first cells assembled on the designated aluminum rack. c) all the cells reassembled and final operations on the head of the battery.

To preserve the membranes to dry up, they were stored in a sealed and humified box and the piling procedure was performed during one single day of work.

At first, every hole of the manifold on each plate was accurately checked and inspected to eliminate any possible leftovers which could occlude them and invalidate further tests. During this check, plate 16 was found to have a consistent part of its holes occluded due to a construction damage. This plate's status could be responsible for the drastic fall in voltage registered in some cases while discharging. Figure 6.11 shows the plot of voltage versus time of the cells and the fall of cell 16 is pointed. As a matter of facts, if not enough reagents are feed to the cell, the resistance rises, and the voltage drops if the current is constant.

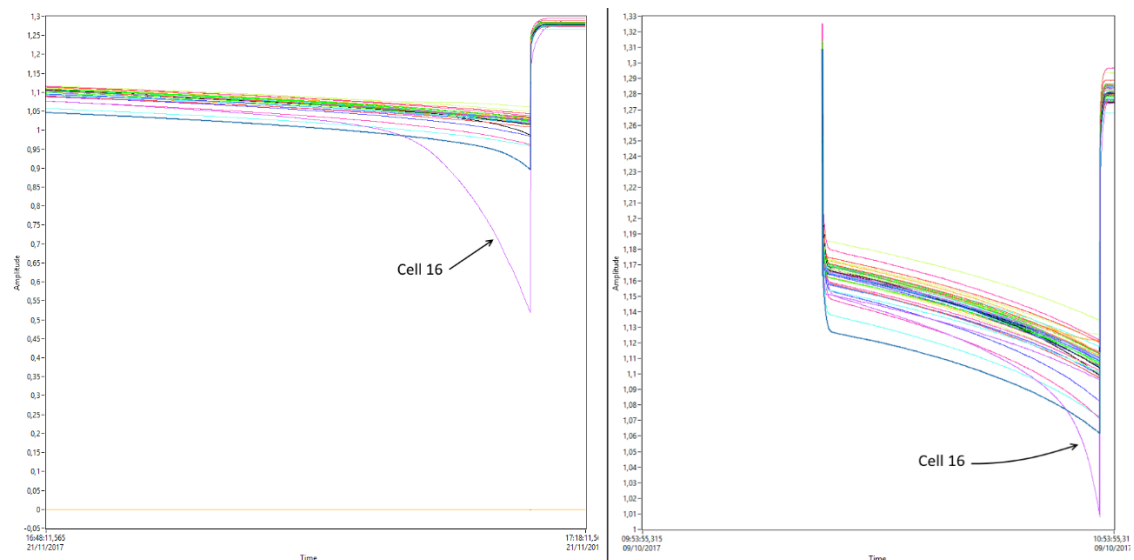


Figure 6.11 Voltage vs time graph of the stack's cells. Cell 16's behavior is pointed.

All the occlusions have been removed successfully and the plate restored to its standard conditions. After that, the stack was reassembled in the exact same order by heaping bipolar plates, electrodes and membranes. Figure 6.10 shows the described phases. Plates 17 and 34 have been replaced with new ones due to a consistent separation between the two halves which can compromise the battery's future performances.

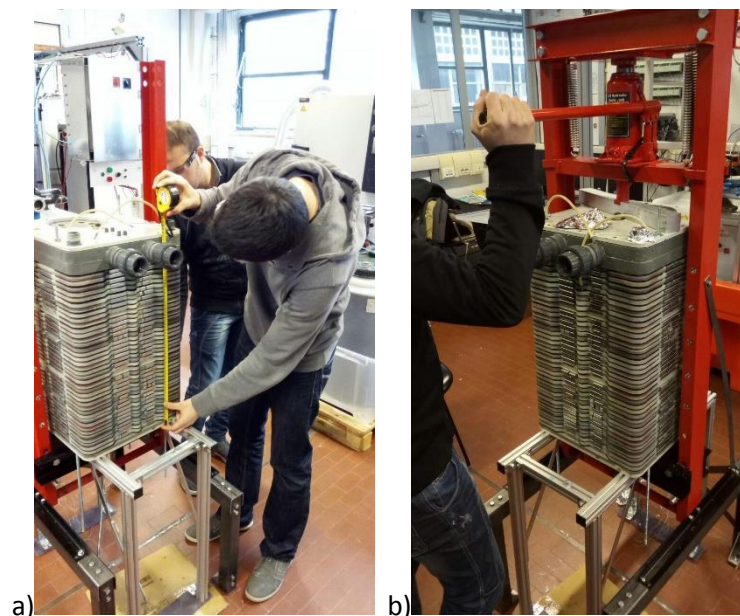


Figure 6.12 Stack measuring and pressing.

After all the components were set in position, the red press together with the aluminum rack were used to press the stack to its original dimensions. Periodic measurements were performed to verify the total length. Finally, a manual and more precise pressing was done with the threaded bars on the perimeter of the stack.

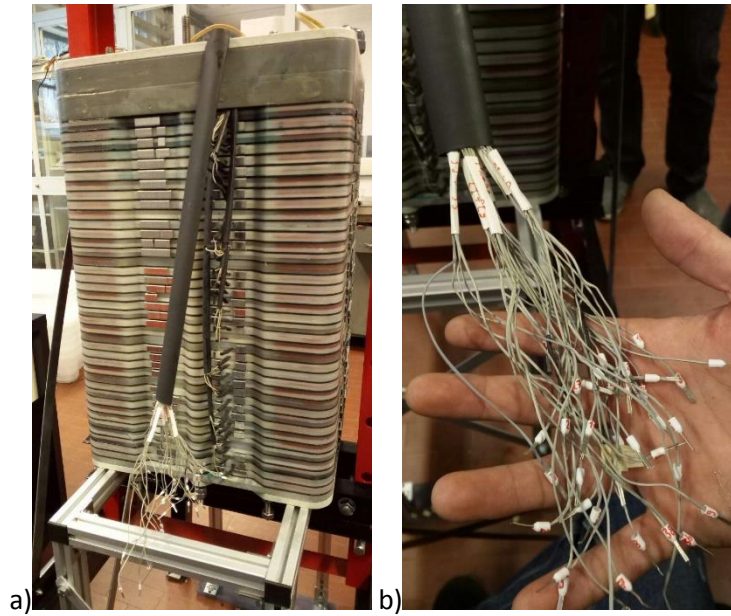


Figure 6.13 Single cells cabling.

When the stack reached its original dimensions all the cablings of the single cells were restored and marked as shown in Figure 6.13. Then, with the yellow crane, the stack was moved, set horizontal and mounted in the original position.

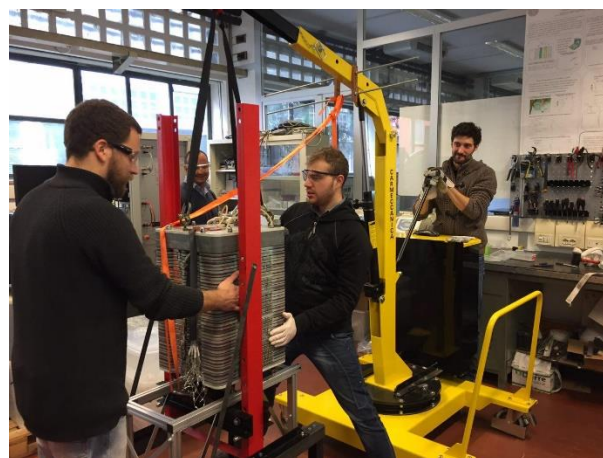


Figure 6.14 The stack is repositioned horizontal.

As a final operation a gas tightness test was done using soapy water to detect eventual leakage by the formation of soap bubble. No outflows were observed when up to 0,5 bar of nitrogen were injected in the stack.



Figure 6.15 The gas tightness test.

After all the piping were restored, the maintenance procedure was concluded, and the test facility was ready to proceed with the experiments.

7 Conclusions

The VRFB test facility located in the Energy Storage Laboratory needs a complex system for its management and data acquisition due to the large amount of measurements and parameters to be controlled. Thanks to a LabVIEW management system which had already been developed when this work began, it is possible to keep under control the whole apparatus. One of its features is the possibility to continuously modify and improve its structure based on state machines so that, in this thesis work, two main routines have been introduced to expand the program's data acquisition capabilities. Thanks to a LabVIEW routine and a Matlab code, it is now possible to plot complete polarization curves giving the user the possibility to set all the necessary parameters. A first and preliminary data acquisition campaign produced the results that are here reported while a second and more accurate one is under way. Moreover, another routine was written and implemented for the calculation of efficiencies. Since these automations are inserted in parallel to others, it is possible to keep checking all the battery parameters and computing the efficiency of the process while charging or discharging. Another LabVIEW feature is the division between the code environment, where the program is developed, and the user interface. The latter is a graphic front-end that can be personalized and gives the user a complete overview on the measurements and the control over routines and procedures. Both these parts were rearranged during the thesis with the introduction of substructures to simplify the comprehension of the code and to make the user interface more user-friendly. Some of the ancillary work focused on the prevention of risks, with the insertion of additional safety devices for the plant, on the creation of a complete electric cabling scheme, to allow easy maintenance and modification of the hardware structure, and on the enhancement of measurements by the elimination of electromagnetic noise. This last work is a part of the experimental activities which included the construction of a metal shielding, the choice of adequate cables and the installation of filters which preserved the measurements from interferences. The main experimental activity during the work is represented by the one-year Maintenance Repair and Operations procedure. Its purpose was to check the status of the stack components like plates, electrodes and membranes and to research the cause of some flaws and leakages detected during normal working conditions. Except for some secondary and non-prejudicial defects, no severe damage has been detected and the stack has been reassembled and remounted. Two bipolar plates have been substituted as a precaution to prevent electrolyte leakages from imperfect sealings. Other experimental activities included the construction and cabling of a passive load and some

ordinary maintenance. Finally, a preliminary study has been carried out over the electrolytes behavior and thermal stability to create a more accurate temperature control during the stand-by of the plant which is still under development. The data presented can be the beginning for future works to enhance the performances of the test facility.

8 Figure Index

Figure 1.1 Graphical representation of Discharge Time vs. Power for the main ES technologies. Some of them are already available other are under development. [1]	1
Figure 1.2 General structure of a VRFB cell with all its fundamental components. [1]	6
Figure 1.3 The MEA. A single cell's structure. [3]	7
Figure 1.4 Parallel Feeding for a VRFB. It is depicted just the circulation of one of the two electrolytes	8
Figure 1.5 . VRFB costs breakdown for materials and ancillaries. [11]	11
Figure 2.1 Vanadium Redox Flow Battery - Industrial Scale Experiment logo	13
Figure 2.2 Energy Storage Lab VRFB-IS main components. A) the Computer with the LabVIEW software user interface, B) opto-isolators, CompactDAQ and other acquisition instruments, C) the VRFB test facility complete with all the measurement equipments, D) Electric panel and power sink selector panel, E) the power supply.	13
Figure 2.3 P&ID of the hydraulic plant in detail.	15
Figure 2.4 Differential pressure gauge detail	16
Figure 2.5 Acquisition core system.	17
Figure 2.6 Volumetric Flow meter.	17
Figure 2.7 Working principle of the E+H flow meter. [14]	18
Figure 2.8 Differential Pressure meter with its dedicated pressure line.	19
Figure 2.9 Wattmeter and electric connections scheme.	20
Figure 2.10 Electric wiring scheme of module NI 9207 for the acquisition of analog inputs, in the connections color of cables and number of pins are highlighted.	21
Figure 2.11 Electric connection of the measurement system. Electric schemes of the NI modules are drawn.	22
Figure 2.12 Electric scheme of the power connections. On the left it's shown the grounding connection of the inner and outer structure which sustain the stack	23
Figure 2.13 PLC connections.	25
Figure 2.14 Micro-switch security system	26
Figure 2.15 Inverter-motor cable section. Courtesy of [16].	27
Figure 2.16 Copper shielding pipes for motor-inverter cables.	27
Figure 2.17 Electromagnetic shields examples. [17]	28
Figure 2.18 Shielding metal box.	28

Figure 2.19 LabVIEW interface Block Diagram. a) Initialization, b) Error Case Structure (Program's main core), c) Final Sequence	30
Figure 2.20 LabVIEW interface Front Panel.....	33
Figure 2.21 An example of how the adoption of SubVI can clarify the view in the block diagram. The block diagram in the case "Efficiency" before a) and after b) the use of a SubVI.	36
Figure 2.22 LEM current transducer SubVI logo.	36
Figure 2.23 Graph for the calibration of the LEM current transducer. It plots the difference between the current from the transducer and the one from the shunt resistor as a function of the current from the transducer.	37
Figure 2.24 LEM calibration SubVI structure.....	38
Figure 2.25 OCV to SOC SubVI logo	38
Figure 2.26 State of Charge % as a function of the Open Circuit Voltage computed with the theoretical formula at 25 °C.	39
Figure 2.27 Block Diagram of the routine to convert OCV into SOC.	40
Figure 2.28 State of Charge tank indicator in the front panel.	40
Figure 2.29 Integral Efficiency SubVI logo.	40
Figure 2.30 Block Diagram of the integral efficiency SubVI	41
Figure 2.31 α -factor SubVI logo.....	42
Figure 2.32 The two cases of the alfa-factor SubVI. a) in case of Charge refers to equation (15), b) in case of Discharge uses equation (16).	43
Figure 3.1 A general polarization curve.....	45
Figure 3.2 a) The firstly used variable resistor as a parallel of 12 variable resistors. The switches and the cursors permit the regulation of different configuration to reach the desired value of resistance. Its value depends by the configuration and connection adopted. $R=15\ \Omega$ for each resistor. b) Detail of the cursor.	46
Figure 3.3 a) Contactors panel and cabling, b) front panel complete of switches and LEDs for load switching, c) details of the user selector panel in operation.	47
Figure 3.4 Electrical scheme of the load selector. Green cables are the control cables while blue cables are the power cables. 1 is the bipolar contactor to allow conduction, 2 and 3 are the tripolar contactors that switches from the passive load to the power supply.	48
Figure 3.5 Passive load. Four variable resistors composing the load. On the right a particular of the slider to adjust the resistance.	48
Figure 3.6 Polarization Settings SubVI logo.....	49
Figure 3.7 a) the Polarization case in the UI Handling loop, b) the window that allows the user to set the parameter for the polarization routine, c) the SubVI internal structure.	50

Figure 3.8 Flowchart of the automatic procedure to collect data for Polarization Curve computation.....	52
Figure 3.9 Matlab general code which automatically analyses the data collected from LabVIEW.	53
Figure 3.10 Polarization curves, charge, first campaign.	54
Figure 3.11 Polarization curves, discharge, first campaign.....	55
Figure 3.12 Polarization curves for different SOC's.	56
Figure 3.13 Power profiles for different SOC's.	56
Figure 4.1 Efficiency routine flowchart.	60
Figure 4.2 Behavior of SOC (time) for charging and discharging.	64
Figure 5.1 Graphs of induction time as a function of SOC and Temperature following equation (18). a) T = 30 to 60 °C, SOC = 0 to 100%, b) T = 30 to 60°C, SOC = 90 to 95%, c) T = 50 to 60°C, SOC = 90 to 95%.	67
Figure 6.1 a) Plant after the first phase: OCV cell, LEM and horizontal upper profile removed, b) the removed objects accurately separated.	69
Figure 6.2 Second phase: the mixing valve is dismantled from the frontal panel.....	70
Figure 6.3 Aluminum rack and hydraulic pressure jack.	70
Figure 6.4 Third phase: the stack's hung and moved with a crane and placed horizontally.	71
Figure 6.5 Fourth phase: the stack's turned vertically. a) some electrolyte leakage is detected from the bottom part, b) wooden clips are applied to avoid polypropylene plates to open completely as it can be noticed in c).....	71
Figure 6.6 Fifth phase: MEA disassembled and preliminary visual check. In b) some manifold channels are blocked up by PVC shavings due to previous drilling maintenance operations on the head plate.	72
Figure 6.7 PVC frontal plate is divided from its metal where more electrolyte leakage are detected.	73
Figure 6.8 Seventh phase: each MEA is divided and each bipolar plate is washed with bi-distilled water and accurately examined.....	73
Figure 6.9 Some of the flaws found on the plates. a) a carbon felts' hole, b) acetic silicone behavior in presence of corrosive environment and electric field, c) and d) imperfections on bipolar plates surface, e) and f) carbon felts' deposit close to the plate's inlet.....	75
Figure 6.10 Reassembly procedure's operations. a) a final and accurate check on the manifold's holes status. b) first cells assembled on the designated aluminum rack. c) all the cells reassembled and final operations on the head of the battery.	76
Figure 6.11 Voltage vs time graph of the stack's cells. Cell 16's behavior is pointed.	77

Figure 6.12 Stack measuring and pressing.	77
Figure 6.13 Single cells cabling.	78
Figure 6.14 The stack is repositioned horizontal.	78
Figure 6.15 The gas tightness test.	79

9 Nomenclature

Abbreviations

BOP	=	Balance of Plant
CAES	=	Compressed Air Energy Storage
Capex	=	Capital Expenditure
CompactDAQ	=	Compact Data Acquisition
DoD	=	Deep of Discharge
E+H	=	Endress+Hauser
ECES	=	Electrochemical Energy Storage
EDLC	=	Electric Double Layer Capacitors
EMC	=	Electromagnetic Compatibility
ES	=	Energy Storage
ESLab	=	Energy Storage Laboratory
FES	=	Flywheel
FIFO	=	First In First Out
GV	=	Global Variable
LED	=	Light-Emitting Diode
MEA	=	Membrane Electrode Assembly
MRO	=	Maintenance Repair & Operations
MS	=	Management System
NI	=	National Instruments
NIOSH	=	National Institute for Occupational Safety and Health
O&M	=	Operations and Maintenance

OCV	=	Open Circuit Voltage
P&ID	=	Piping and Instrumentation Diagram
PCS	=	Process Control System
PHES	=	Pumped Hydro Energy Storage
PID	=	Proportional Integral Derivative
PLC	=	Programmable Logic Controller
PV	=	Photovoltaic
PVC	=	Polyvinyl Chloride
RES	=	Renewable Energy Sources
RFB	=	Redox Flow Battery
RMS	=	Root Mean Square
SCES	=	Super Capacitor Energy Storage
SLI	=	Start, Lights and Ignition
SMES	=	Superconducting Magnetic Energy Storage
SOC	=	State of Charge
SPEEK	=	Sulfonated Poly Ether Ether Ketone
T&D	=	Transmission and Distribution
UPS	=	Uninterruptable Power Supply
VRFB	=	Vanadium Redox Flow Battery
VRFB-IS	=	Vanadium Redox Flow Battery – Industrial Size

10 Bibliography

- [1] M. Guarnieri, P. Mattavelli, G. Petrone e G. Spagnuolo, «Vanadium Redox Flow Batteries,» *IEEE Industrial Electronics Magazine*, 2016.
- [2] S. Jaffe, «The Battery Industry. Global Market Sizing and Forecast. Forecast and Supply Chain Analysis.,» *CAIRN Energy Research Advisor*, September 2015.
- [3] P. Alotto, M. Guarnieri e F. Moro, «Redox flow batteries for the storage of renewable energy: A review.,» *Renewable and Sustainable Energy Reviews*, 2014.
- [4] L. Li e et al., «A Stable Vanadium Redox-Flow Battery with High Energy Density for Large-Scale Energy Storage,» *Adv. Energy Mater*, 2011.
- [5] M. Skyllas-Kazacos e M. Kazacos, «State of charge monitoring methods for vanadium redox flow battery control,» *Journal of Power Sources*, 2011.
- [6] B. Xiong e et al., «Thermal hydraulic behaviour and efficiency analysis of an all-vanadium redox flow battery,» *Journal of Power Sources*, 2013.
- [7] L. Arenas, L. Ponce de Leòn e F. Walsh, «Engineering aspects of the design, construction and performance of modular redox flow batteries for energy storage,» *Journal of Energy Storage*, 2017.
- [8] C. Ding e et al., «Vanadium Flow Battery for Energy Storage : Prospects and Challenges,» *The Journal of Physical Chemistry*, 2013.
- [9] M. Skyllas-Kazacos e J. McCann, «10 - Vanadium redox flow batteries (VRFBs) for medium- and large-scale energy storage,» in *Advances in Batteries for Medium- and Large-scale Energy Storage*, Elsevier Ltd., 2015.
- [10] P. Leung e et al., «Progress in redox flow batteries, remaining challenges and their applications in energy storage,» *RSC Advances*, 2012.
- [11] S. Ha e et al., «Estimating the system price of redox flow batteries for grid storage,» *Journal*

of Power Sources, 2015.

- [12] G. Kear, A. Shah e F. Walsh, «Development of the all-vanadium redox flow battery for energy storage: a review of technological, financial and policy aspects,» *Internation Journal of Energy Research*, 2011.
- [13] B. Zakeri e et al., «Electrical energy storage system: A comparative life cycle cost analysis,» *Renewable and Sustainable Energy Reviews*, 2015.
- [14] E. a. H. A. [CH], «www.it.endress.com,» Endress and Houser , [Online]. Available: <https://www.it.endress.com/it/panoramica-strumentazione-da-campo/Misura-di-portata/Promag-50W>.
- [15] Allen-Bradley . Rockwell Software, *Regole generali di cablaggio e messa a terra degli inverter a modulazione di ampiezza degli impulsi (PWM)*..
- [16] Bericacavi Spa, «bericacavi.com,» [Online]. Available: <http://www.bericacavi.com/index.php/4-schermati/92-fg7oh2r-t-0-6-1-kv>.
- [17] D. Desideri, *Lectures 32, 33, 34, 35 - Shielding*, Padova, 2016/2017.
- [18] R. Bitter, T. Mohiuddin e M. Nawrocki, *LabVIEW: Advanced Programming Techniques*, Seconda edizione a cura di, CRC Press, 2007, p. 1.
- [19] R. H. King, *Introduction to Data Acquisition with LabVIEW*, McGraw-Hill, 2009, pp. 7-11,100.
- [20] M. Giacomo, *Attività di commissioning per un impianto sperimentale VRFB*, Padova, 2017.
- [21] Y. Yan, Y. Li, M. Skyllas-Kazacos e J. Bao, «Modellind and simulation of thermal behaviour of vanadium redox flow battery,» *Journal of Power Sources*, n. 332, pp. 116-128, 2016.
- [22] National Instruments, *LabVIEW Core 1 Participant Guide*, 2014.
- [23] A. Tang, J. McCann , J. Bao e M. Skyllas-Kazacos, «Investigation of the effect of shunt current on battery efficiency and stack temperature in vanadium redox flow battery,» *Journal of Power Sources*, 2013.
- [24] D. Oboroceanu, N. Quill, C. Lenihan, D. Eidhin, S. Albu, R. Lynch e D. Noel Buckley, «Effects of Temperature and Composition on Catholyte Stability in Vanadium Flow Batteries :

Measurement and Modeling,» *Journal of The Electrochemical Society*, 2017.

[25] F. Rahman e M. Skyllas-Kazacos, «Vanadium redox battery: Positive half-cell electrolyte studies,» *Journal of Power Sources*, 2009.

[26] M. Kazacos, M. Cheng e M. Skyllas-Kazacos, «Vanadium redox cell electrolyte optimization studies,» *Journal of Applied Electrochemistry*, 1990.